minerals

MDPI

Article

The Açdif Gold-Bearing Shear Zone (Zenaga Inlier, Central Anti-Atlas, Morocco): New Petro-Structural and Geochemical Data

Mohammed El Azmi [1,2], Mohamed Aissa [1], Azizi Moussaid [1], Said Ilmen [3], Hafid Mezougane [1,4,*], Ilya Prokopyev [5], Ilyasse Loudaoued [1], Muhammad Souiri [2], Hassane Ouguir [1], Mohammed Aarab [1], Mohamed Zouhair [2], Lhou Maacha [2] and Safouane Admou [2]

1 Laboratory of Mineral and Energy Resources Studies (LERME), Faculty of Sciences, Moulay Ismail University, M.B. 11201, Zitoune, Meknès 50070, Morocco; moh.elazmi@edu.umi.ac.ma (M.E.A.); mohamedaissa@gmail.com (M.A.); moussaid.azizi@gmail.com (A.M.); i.loudaoued@edu.umi.ac.ma (I.L.); ouguir6162@gmail.com (H.O.); m.aarab@umi.ac.ma (M.A.)
2 Managem Group, Twin Center, Tour A, Angle Boulevards Zerktouni et Al Massira Al Khadra, BP 5199, Casablanca 20000, Morocco; souiri.muhammad@gmail.com (M.S.); m.zouhair@managemgroup.com (M.Z.); l.maacha@managemgroup.com (L.M.); s.admou@managemgroup.com (S.A.)
3 CAG2M, Polydisciplinary Faculty of Ouarzazate, Ibnou Zohr University, Avenue Moulay Ettahar Ben Abdulkarim, BP. 638, Ouarzazate 45000, Morocco; s.ilmen@uiz.ac.ma
4 Physico-Chemistry of Processes and Materials Laboratory, Research Team Geology of the Mining and Energetics Resources, Faculty of Sciences and Techniques, Hassan First University of Settat, Settat 26002, Morocco
5 Sobolev Institute of Geology and Mineralogy, Siberian Branch of the Russian Academy of Sciences, 3 Academician Koptyug Ave, Novosibirsk 630090, Russia; prokopev_ilya@mail.ru
* Correspondence: hafid.mezougane@uhp.ac.ma

Abstract: The Açdif gold deposit is located in the Zenaga Inlier (central Anti-Atlas), approximately 120 km southwest of the city of Ouarzazate. It hosts gold mineralization associated with a shear zone affecting the metamorphic and magmatic formations of the Eburnean basement. It mainly consists of alternating micaschists, augen gneisses, and orthogneiss. These crystalline rock assemblages are intruded by a variety of granitoids. These are the Azguemerzi granitoids, which are locally affected by Eburnean deformation. Subsequently, these facies are intersected by a swarm of mafic dykes, which show a variety of rocks ranging from microgabbro-dolerite to quartz diorite. Detailed mapping, petro-mineralogical investigations, and geochemistry of the major and trace elements of these magmatic intrusions suggests the following: (i) for the granodiorite rocks (deposited before the basic dykes), a calc-alkaline affinity, with a chemical signature similar to a syn-collisional context; (ii) for mafic dykes, a contemporaneous emplacement of these mafic intrusions with an evolutionary process controlled by fractional crystallization of the same magma of continental tholeiites, whose chemical composition is comparable to that of enriched MORBs (EMORBs). These continental tholeiites are related to a distensive tectonic context that would have affected the Zenaga inlier prior to the Pan-African orogeny.

Keywords: granitoids; mafic dyke; continental tholeiites; Açdif; Zenaga; Anti-Atlas; Morocco

check for updates

Citation: El Azmi, M.; Aissa, M.; Moussaid, A.; Ilmen, S.; Mezougane, H.; Prokopyev, I.; Loudaoued, I.; Souiri, M.; Ouguir, H.; Aarab, M.; et al. The Açdif Gold-Bearing Shear Zone (Zenaga Inlier, Central Anti-Atlas, Morocco): New Petro-Structural and Geochemical Data. *Minerals* **2023**, *13*, 1116. https://doi.org/10.3390/min13091116

Academic Editors: Huan Li and Paris Xypolias

Received: 20 June 2023
Revised: 23 July 2023
Accepted: 8 August 2023
Published: 24 August 2023

Copyright: © 2023 by the authors. Licensee MDPI, Basel, Switzerland. This article is an open access article distributed under the terms and conditions of the Creative Commons Attribution (CC BY) license (https://creativecommons.org/licenses/by/4.0/).

1. Introduction

The West African Craton (WAC) preserves several Paleoproterozoic basement terrains [1] (supercontinents), which host a significant number of magmatic intrusions of different natures and ages. These magmatic formations outcrop in several inlier structures of the Anti-Atlas. The Zenaga inlier, located south of the major Anti-Atlas fault (AAMF), hosts some of the oldest of these intrusions. This part of the West African Craton, which has remained stable since the end of the Lower Proterozoic [2], is bordered to the north by the Pan-African arc [3] and to the south by Eburnean outcrops. The Paleoproterozoic

formations in this inlier include stratified supracrustal schists, gneiss, and migmatites, so-called the Zenaga Complex [4]. These are ancient metamorphozed volcanic–sedimentary formations that are intruded by various plutonic rocks, mainly granites, and granodiorites. The previous dating works on the Zenaga massif attributed these intrusions to the Eburnean orogeny. The granitic masses were dated by [5] on the Assourg tonalite (2037 ± 7 Ma), the Azguemerzi granodiorite (2032 ± 5 Ma), and the Tazenakht granite (Tamazzarra) (2037 ± 9 Ma). In [6], the authors connect these granites and the swarm of mafic dykes (dated 2040 ± 2 Ma to 884 ± 28 Ma) to the first extensional magmatic event in the Anti-Atlas.

The entire inlier is affected by a brittle tectonic that facilitated its dislocation and the injection of a swarm of mafic dykes and veins along subvertical fractures [7]. These mafic dykes are considered as continental tholeiites [8]. They are comparable with other dykes of the same age in other inliers of the Anti-Atlas (Tagragra of Akka, Iguerda-Taïfast, and Agadir Melloul) [9]. The absolute dates recently made on the different types of mafic dykes of the Zenaga inlier, show a variation in ages, ranging from 2043 Ma to 887 Ma [6,9]. The spread of the ages of these formations over such a long period (2043–887 Ma) leaves questions remaining about the establishment of these dykes. The Açdif gold deposit is located in the south-western part of the Zenaga inlier. The deposit is actually mined for its gold resources which are occurring in the ENE-WSW trending structural shear zone. This later cuts the Azguemerzi granodiorite, schists, and mafic dykes. This work provided new petrographic, structural, and geochemical data of these magmatic formations in the Açdif sector that will contribute to a better understanding of the geodynamic context of the implementation of granitoids and the mafic dykes of the Zenaga inlier.

2. Geological Context

The Açdif shear zone (ASZ) is one of the most gold-bearing deposits in the Zenaga inlier, with a mineral reserve of around 500,000 tons at 1.20 ppm Au. It is located in the Anti-Atlas domain of Morocco, which is part of the northern border of the West African Craton (WAC) (Figure 1). The geology of the Zenaga inlier is mainly composed of a Paleoproterozoic basement, comprising mica schists, gneisses and migmatites, called the Zenaga complex [4] (Figure 2).This unit is intruded by Eburnean-aged granitic intrusions. The main ones are the porphyroid granodiorite of Azguemerzi (2032 ± 5 Ma) and the Tazenakht monzogranite (2037 ± 9 Ma) [5]. Subsequently, all these Paleoproterozoic formations and their calcareous-quartzitic (Taghdout Group) covers of Neoproterozoic age are intersected by a swarm of mafic dykes and sills of a doleritic to gabbroic nature ([8], this study). Ref. [10] considered this set as the sequel to Ifzwane suite. They are grouped into two major directions: N-S to NW-SE and NE-SW to E-W [8] (Figure 2). Recent dating carried out on this magmatism by [6,9] gave an age of 1734 ± 5 Ma using the U-Pb method on baddeleyite minerals. This mafic magmatic activity is also manifested in the inliers of Bas Drâa and Tagragra of Akka [11,12], Agadir Melloul [13], and Iguerda-Taïfast [9]. All the studies carried out on this magmatism [8–10,14] confirm its bimodal character and affinity for continental tholeiites [8] in relation to a pre-Pan-African distensive tectonic phase that affected the Zenaga inlier and the entire West African Craton [15–18].

Structurally, the Palaeoproterozoic formations of Zenaga (granites and their metamorphic host rocks) are affected by two major orogenies, namely, the Eburnean and Pan-African orogenies, which are characterized by the deformation phases D1, D2, and D3. Phase D1 is associated with the Eburnean orogeny, while the sinistral shear regime of phase D2 and the crumpling of phase D3 correspond to the Pan-African orogeny. The latter phase (D3) is manifested by flow schistosity and a regional foliation, locally associated with mylonites. This is the result of a dominant sinistral shearing that affected the northern border of the West African craton [19,20].

The first phase of deformation (D1) shows a submeridian direction and affects the mica-schist basement. During this phase, foliation (S1) is more or less parallel to S0 stratification. The second phase of deformation (D2) of NE-SW direction is considered the main Eburnean

phase, and it was manifested by the appearance of a new foliation and orthogneiss [19]. At the base, it is expressed in the form of penetrative flow schistosity S2, with a direction close to NW-SE with a vergence towards the SW. The last Eburnean phase (D3) is expressed in the Zenaga inlier by a localized migmatization in Azguemerzi granodiorite. As for the Pan-African deformation, it manifested itself in the Zenaga inlier in three main phases. The transpressive phase (D1) of direction NNE SSW is documented north of the inlier, and in the granites of Tazenakht, by the development of mylonites and ultramylonites of the general direction of foliation N 125°–N 140° moderately sloped towards the SW with an SSW lineation. During this phase, the foliation (S1) is parallel to the S0 stratification. The second phase (D2) is a compression phase of submeridian direction. This phase is responsible for the appearance of migmatites and stepped potassium feldspar porphyroblasts in granites as well as documented forms of boudinage at the large Tifri quartz vein linked to Tazenakht granite. The third phase (D3) is characterized by a subhorizontal axis crenulation schistosity. It is synchronous with the emplacement of granite and late Pan-African rhyolites (granite of Sidi El Hosseine and rhyolites located at the northwestern part of the Zenaga inlier) [19].

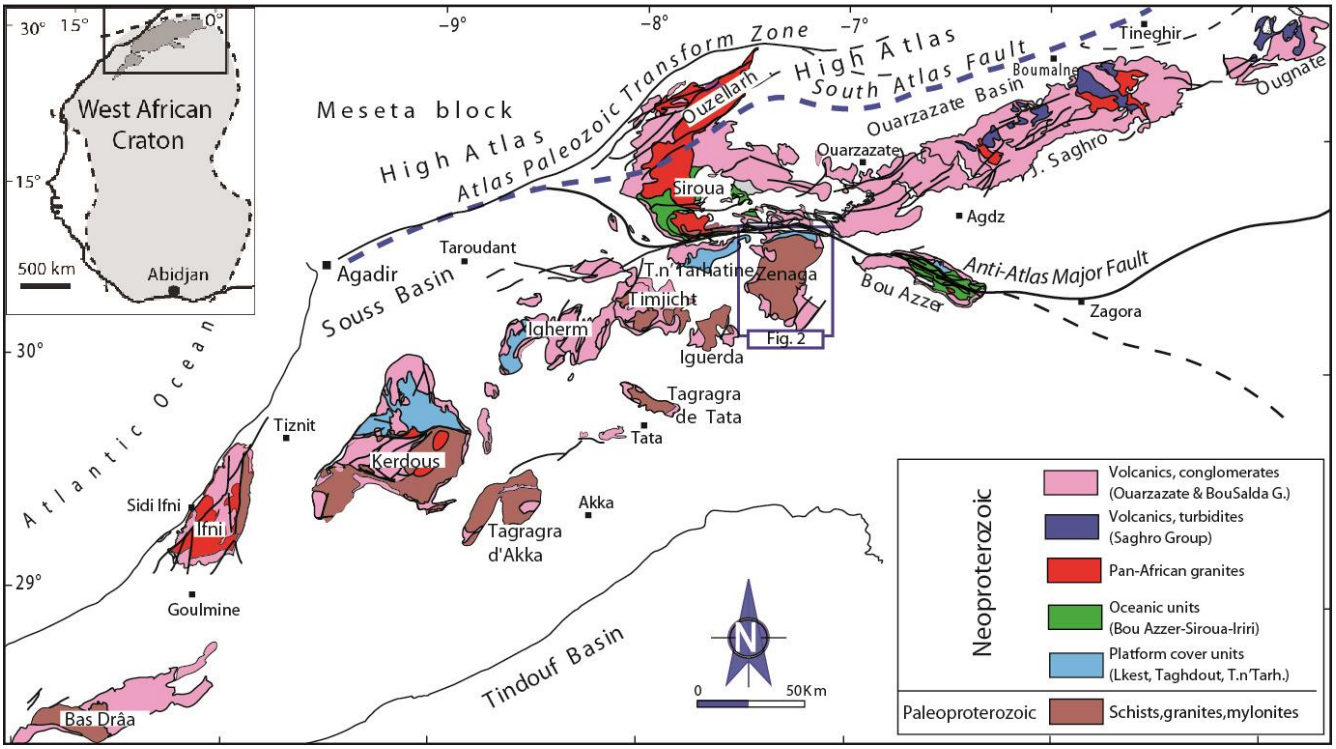


Figure 1. Geological map of the Anti-Atlas belt at the northern margin of the West African Craton (WAC) showing the location of the studied area (modified from [21]).

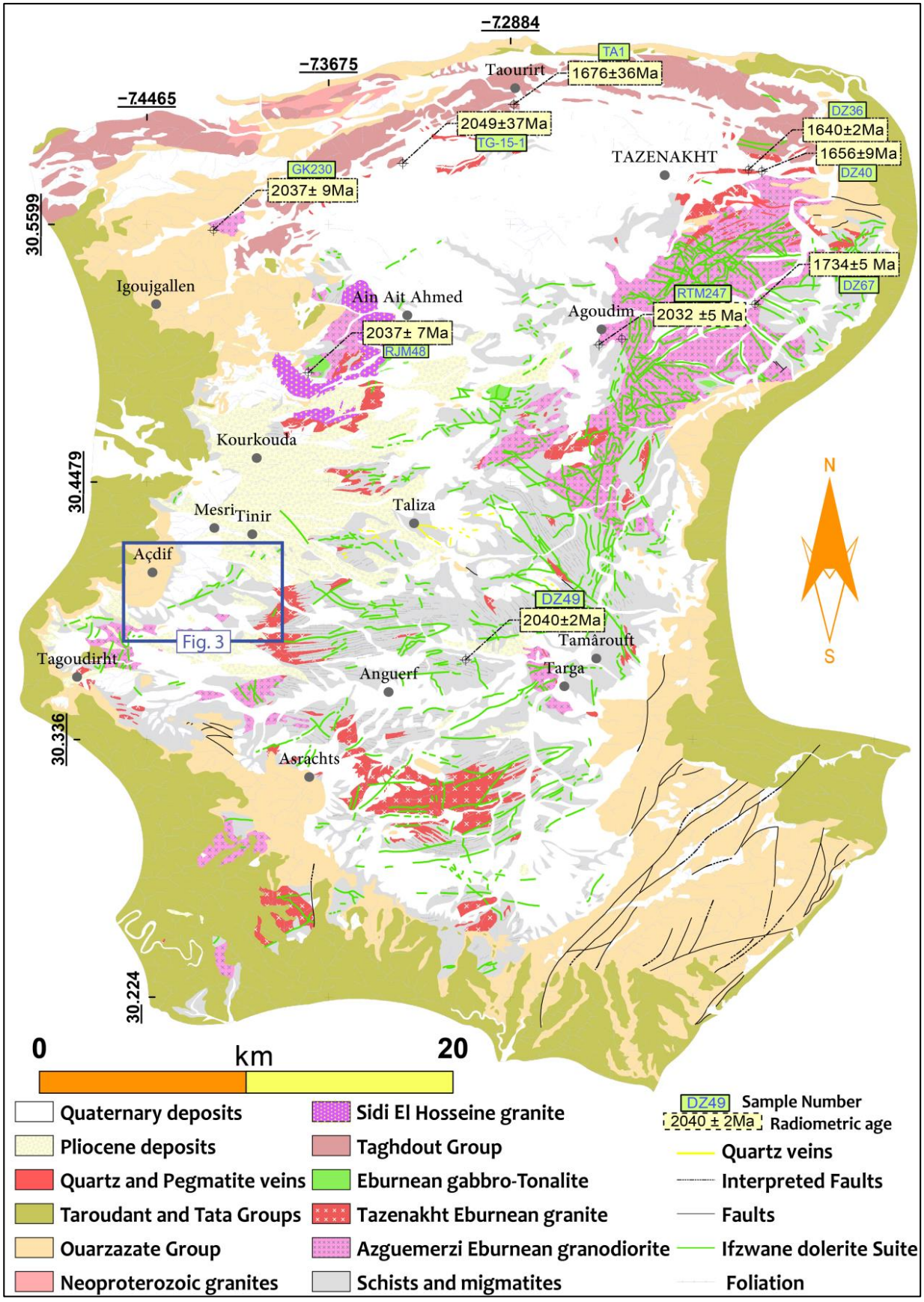


Figure 2. Geological map of the Zenaga inlier and geographical location of Açdif area (modified from [4,10,22]).

3. Materials and Methods

The fieldwork consists of geological mapping, diamond drill core surveys and sampling of the rocks of the different magmatic and metamorphic facies. The sampling concerns the rocks surrounding the mineralization, both mafic dykes, magmatic intrusions, and metamorphic rocks. Ninety thin sections, performed on samples collected from surface and drill cores, have served for petrological and textural studies at the Department of Geology, Faculty of Sciences (Moulay Ismail University, Meknès, Morocco). Ten samples of least-altered rocks were prepared and analyzed for the multi-elements (major, traces and REE) at the Research Center of the Russian Academy of Sciences (Novosibirsk, Russia). Whole-rock compositions were determined via X-ray fluorescence (ARL-9900-XP). Trace and REE element analyses conducted via ICP-MS were performed using a Finnigan MAT under standard operating conditions (open acid digestion using a HF, HNO_3, and $HClO_4$ mixture). The detection limits were determined using 3σ criteria of the blank and ranged from 0.005 up to 0.1 μg/g for a majority of elements. The investigations were carried out at the Analytical Center for Multi-Elemental and Isotope Research Siberian Branch, Russian Academy of Sciences (Novosibirsk, Russia).

Fifteen other samples were prepared and analyzed in the laboratory of the Reminex research center (Managem group, Marrakech, Morocco). The main major elements were analyzed via X-ray fluorescence spectrometry (XRF), while trace and rare earth elements (REE) were analyzed via mating plasma mass spectrometry (ICP-MS).

The WGS 1984 geographic coordinate projection was used to reference the maps of Figures 1 and 2, while the Lambert metric coordinate projection for southern Morocco was used to reference the geological map of the studied area.

4. Results

4.1. Petrography and Lithology

The ASZ is encased in the magmatic and metamorphic formations constituting the Paleoproterozoic base of the Zenaga inlier. Geological mapping work has covered a significant portion of the Açdif deposit district, and the development of a detailed geological map (Figure 3) has facilitated the distinction of several lithological facies:

1. Orthogneiss: Greyish to blackish rock with quartz phenocrysts, potassium feldspar, biotite, and garnet. The latter has rounded porphyroblastic crystals of millimeters in size (Figure 4A,B). On some outcrops, the rock shows a clear foliation with metamorphic bedding (Figure 4A,B). Under the microscope, the orthogneiss shows a paragenesis formed by the following: (i) Quartz: 2 types of quartz are dissected: quartz 1 (Qz1), which is expressed in oval inclusions associated with biotite grains in the garnet that corrodes it (Figure 4C,G), and quartz 2 (Qz2), which has a recrystallization texture (Figure 4C–F,H) with rolling extinction observed on some grains. (ii) Plagioclases show a granoloblastic texture with recrystallization figures. They are severely altered in sericite, which makes their identification difficult. Locally, they show polysynthetic twins (Figure 4E). (iii) The poeciloblastic texture of orthogneiss show garnets as being porphyroblastic in shape (Figure 4A). They have oval inclusions of quartz and biotite (Figure 4C,G) and show two shapes: one is rounded, indicating a syn-tectonic formation, and the other is flattened, indicating greater deformation, with an orientation parallel to the foliation axis (Figure 4D,H). In some cases, garnets appear to be entirely obliterated, with only a few remnants of a porphyroblast that has disintegrated due to deformation stress. Biotite, muscovite, zircon, and opaque mineral grains are incidentally present in these facies (Figure 4F–H). Biotite occurs either as inclusions within garnets or as small flakes elongated along the foliation planes. Opaque minerals primarily correspond to sulphides and iron oxides.

2. Granodiorite of Azguemerzi: This appears dark in color to the naked eye, exhibits a well-crystallized grainy texture (Figure 5A). Microscopically, this facies displays an intense phyllitic alteration, characterized by sericite and muscovite. The texture is porphyritic, composed of phenocrysts of plagioclase, quartz, and potassium feldspar. Plagioclases are mostly sericitized, and quartz is deformed with rolling extinction (Figure 5B,C,E). Small

xenomorphic crystals of these minerals are also present at the interstitial spaces. Potassium feldspars are abundant, particularly in contact with plagioclases (Figure 5C). Rare green hornblende crystals are present in this facies (Figure 5F). Incidentally, zircon and micas are recognizable in this facies (Figure 5B,D).

3. Quartz Microgabbro-Diorite: These facies are part of the Ifzwane suite, and are in the form of a swarm of dykes with different trending directions. This rock shows a centripetal evolution from mafic facies to a quartz dioritic facies. The mafic term of this facies is represented by a microgabbro that is composed of the following: (i) Plagioclases are present in large acicular slats and recognizable by their typical polysynthetic twins. Some sections of this mineral show an onset of alteration (sericite and epidote) (Figure 6C,F); (ii) Clinopyroxene is present with a strong relief and a clear oblique extinction. The crystals appear either as xenomorphic sections filling the interstitial spaces between the plagioclase laths, or as automorphic sections of fairly large size and showing an oblique extinction. The sections of this mineral often exhibit an alteration in chlorite and/or actinote amphiboles (Figure 6B–D). (iii) The abundant amphibole shows automorphic crystals with typical cleavage and is often formed due to pyroxene alteration (ouralitization). Incidentally, rare biotite grains are present in aggregates, often associated with opaque minerals. The evolved portion of this facies is represented by quartz diorite, which corresponds to a porphyritic facies, characterized by a dark color, well-crystallized grainy texture. It displays significant phyllitic alterations materialized by chlorite and sericite (Figure 7A).

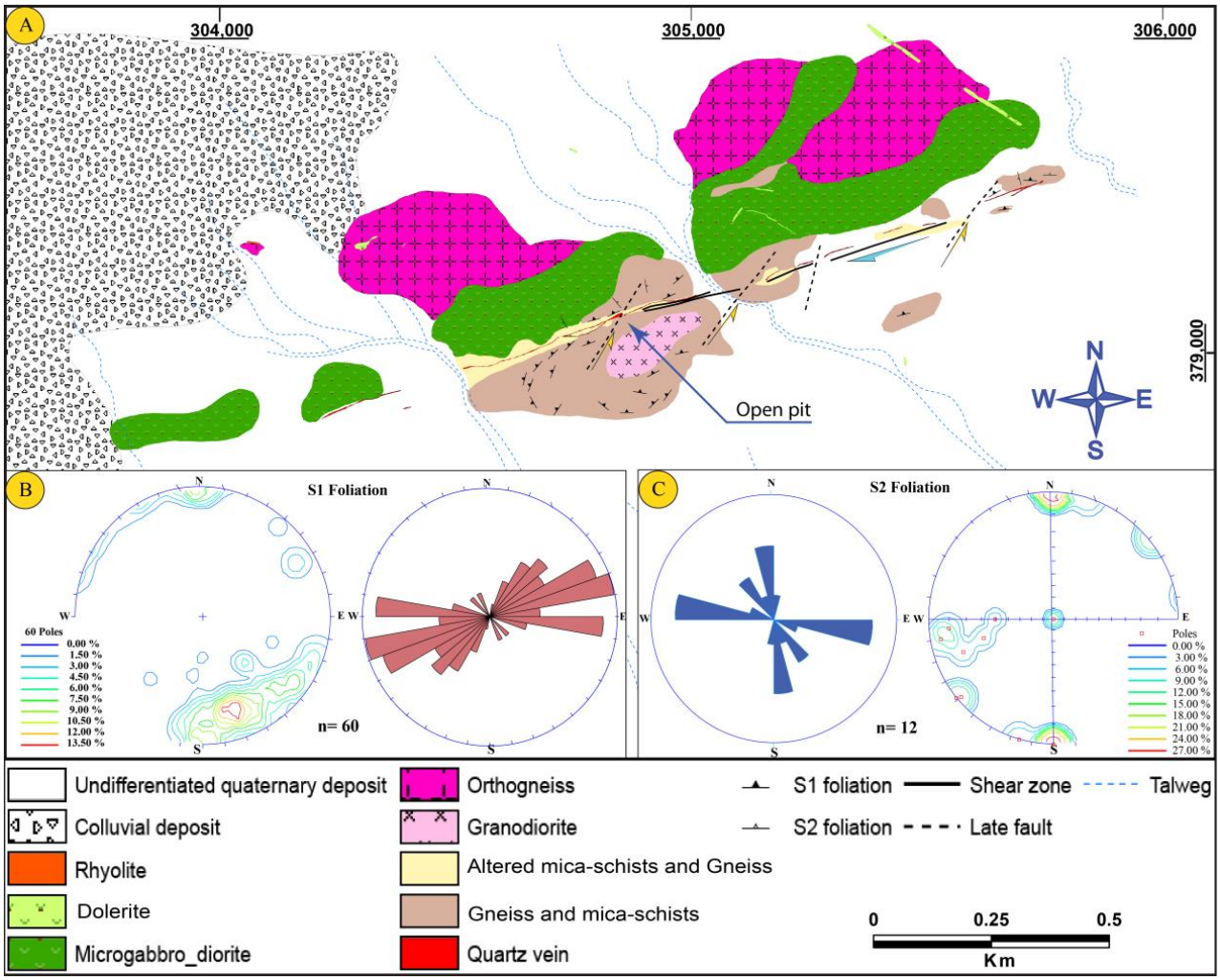


Figure 3. (**A**) Detailed geological map of the Açdif gold deposit. (**B**,**C**) Rose diagrams showing directional and statistic structural measurements of S1 and S2 foliation planes.

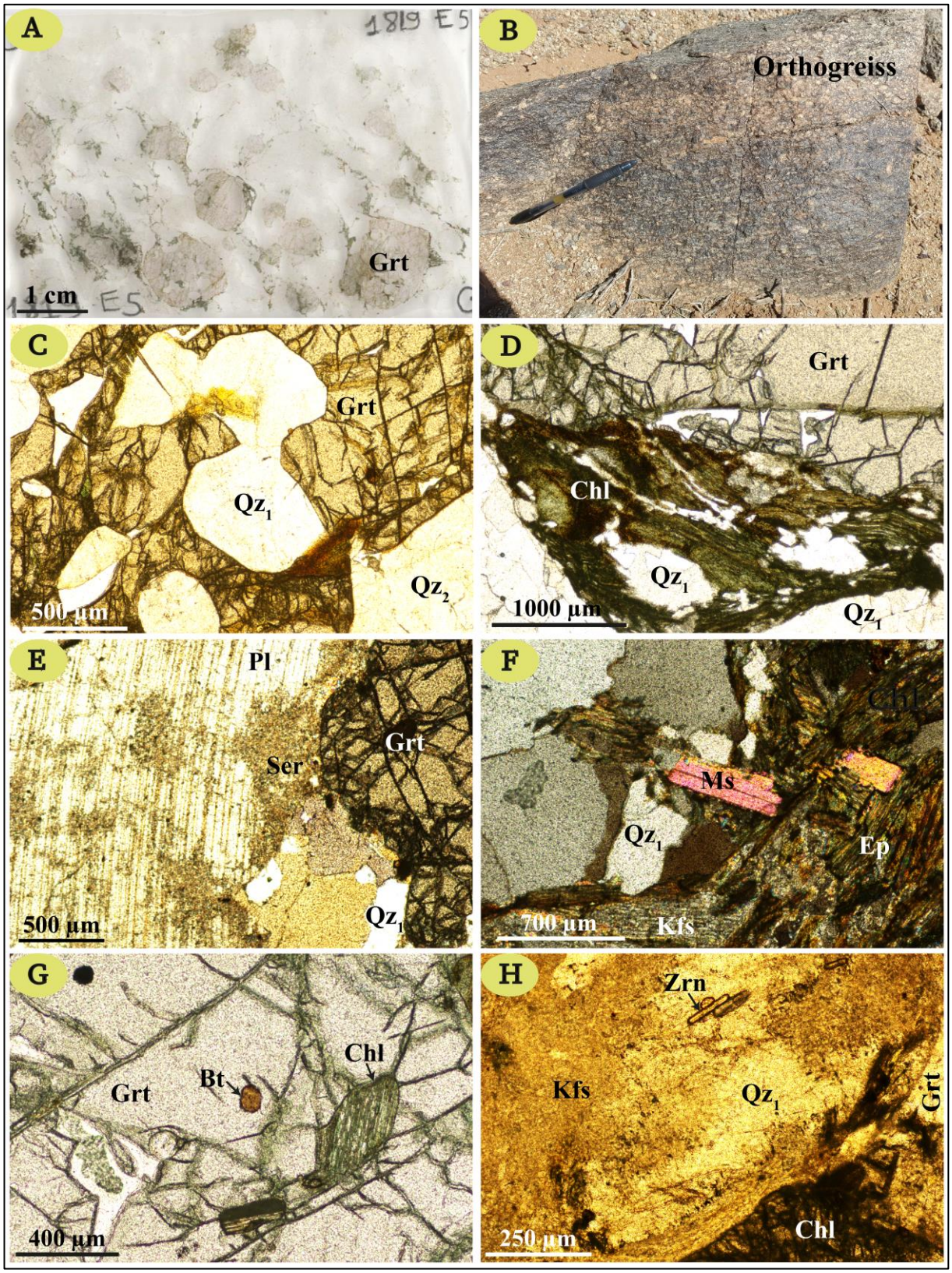


Figure 4. Microphotographs showing mineral paragenesis of the orthogneiss facies: (**A**,**B**) Macroscopic aspect of the orthogneiss; (**C**,**G**) Inclusions of quartz and biotite in the garnet (PLNA); (**E**) Sericitized plagioclases (PLNA); (**D**,**F**,**H**) Mineral paragenesis of the orthogneiss ((**F**) PLN; (**D**,**H**) PLNA). Grt: garnet; Bt: biotite; Ms: muscovite; Pl: plagioclase; Zrn: zircon; Qz: quartz; Kfs: K-Feldspar; Chl: chlorite; Ep: epidote; Ser: sericite.

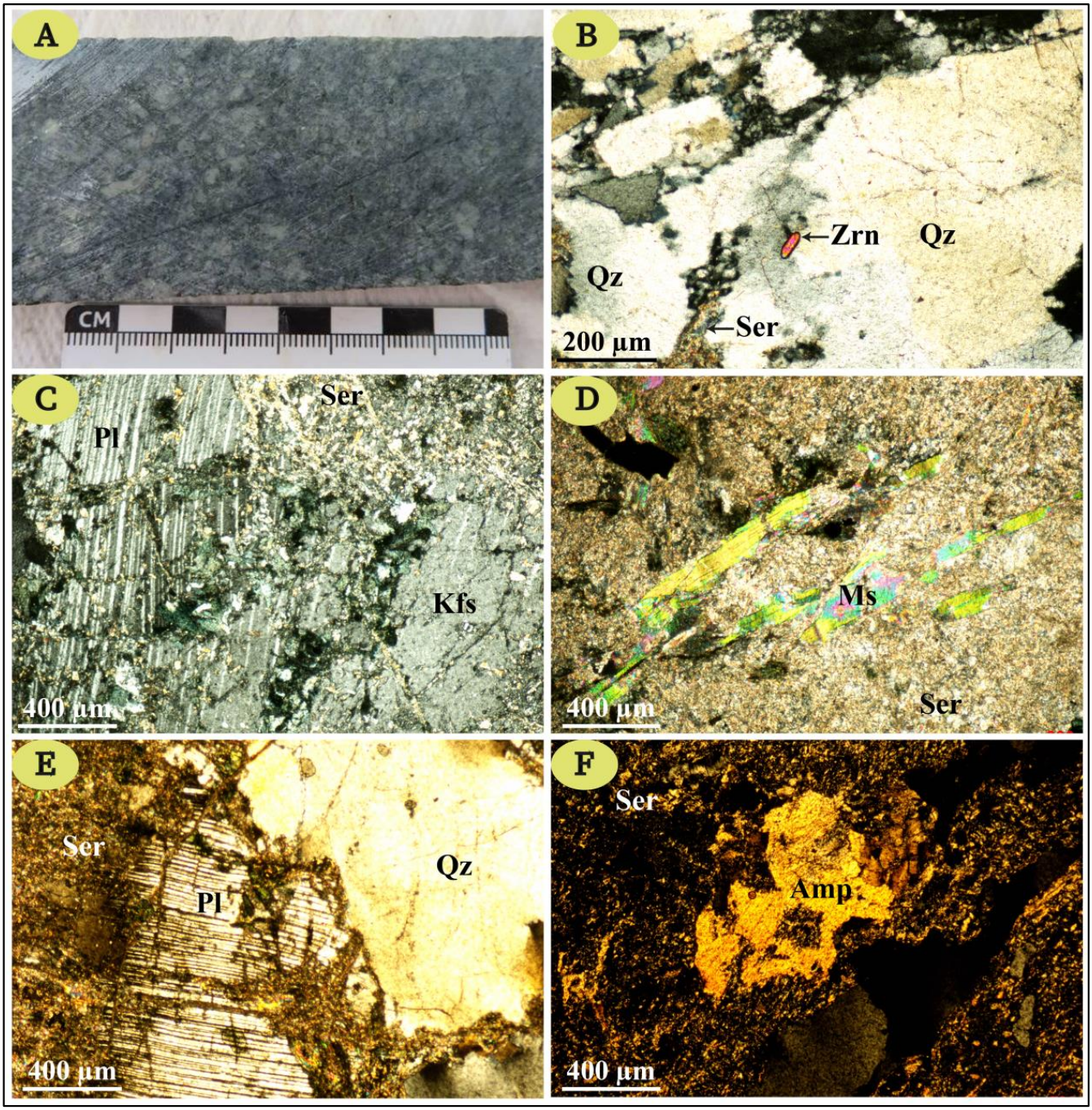


Figure 5. Microphotographs showing the mineral paragenesis of the Açdif granodiorite: (**A**) Macroscopic aspect of the granodiorite; (**B**,**D**) Zircon and muscovite minerals in the granodiorite (PLA); (**C**,**E**,**F**) Mineral paragenesis of the granodiorite ((**C**,**F**) PLA; (**E**) PLNA). Grt: garnet; Ms: muscovite; Pl: plagioclase; Zrn: zircon; Qz: quartz; Kfs: K-Feldspar; Ser: sericite; Amp: amphibole.

In the shear zone area, this facies is intensely deformed and has an appearance of protomylonite (beginning of gneissification), with an alternation of light bands and dark bands. Microscopically, it is composed of the following: (i) k-Feldspath of the orthose type, recognized by its very frequent Carlsbad twins; (ii) plagioclase laths, with a size of less than 3 mm, generally altered into sericite (Figure 7C,E); the largest grains of these plagioclases contain inclusions of amphibole, biotite, epidote, chlorite, and apatite; (iii) amphibole, which is more abundant and shows automorphic crystals; it is a green amphibole of the hornblende type (Figure 7E); (iv) quartz, of variable size and shape, which often occurs in

the form of xenomorphic grains that cement intergranular spaces (Figure 7B); small grains of zircon, biotite, apatite, chlorite, calcite and magnetite are commonly present.

4. Dolerite: These outcrops appear as dark color, fine-grained rock with a compact appearance (Figure 8A). Microscopically, its mineralogical composition includes plagioclases, pyroxenes, and iron oxides (opaque) (Figure 8B–D). This facies is more or less an altered facies, and only plagioclase laths are visible and constitute an important part of the rock volume. They are often altered and replaced by sericite. Pyroxenes are transformed into secondary amphibole and chlorite and they are only recognizable by their relics.

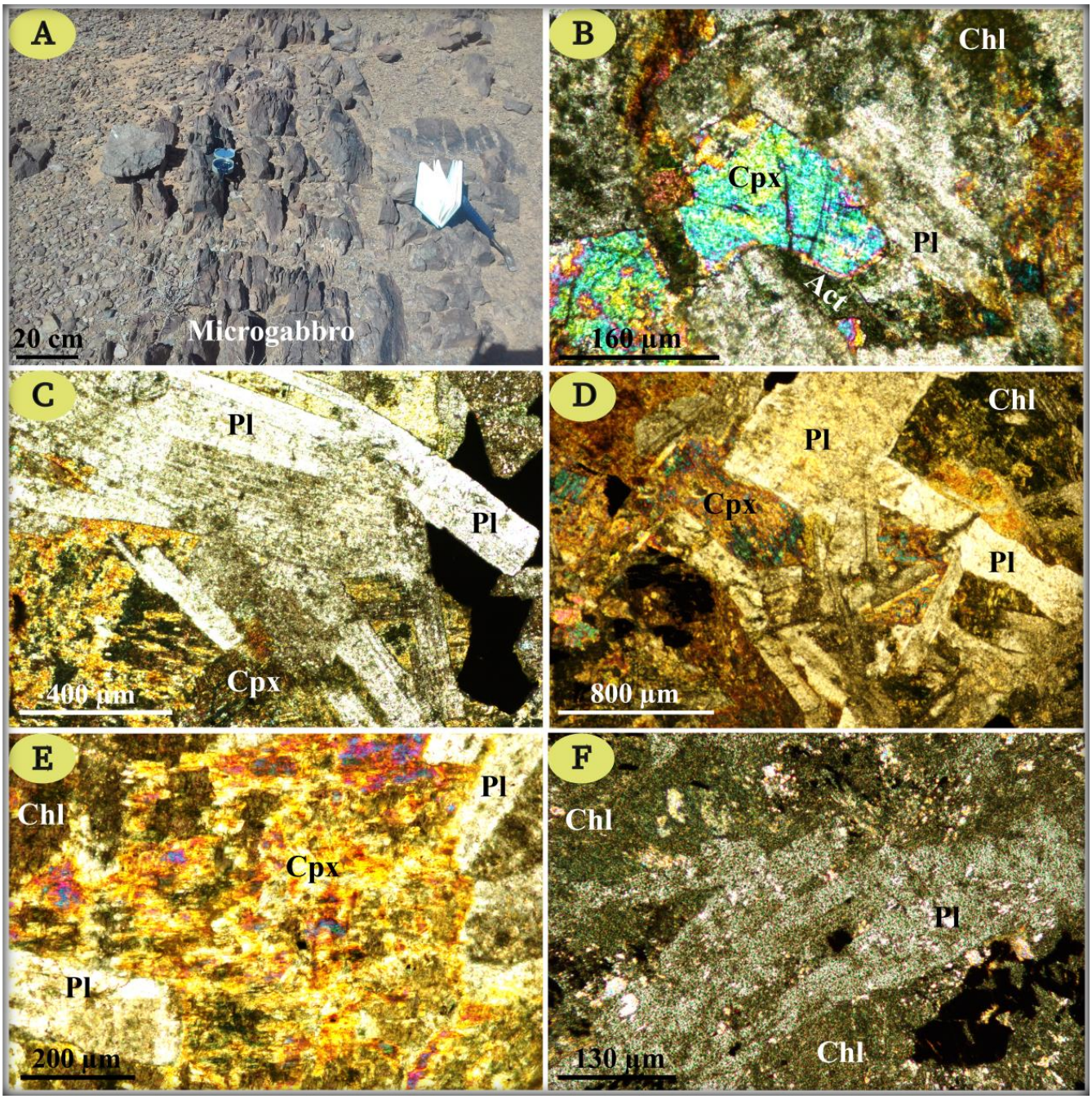


Figure 6. (**A**) Field pictures of the microgabbro. (**B**–**F**) Microphotographs showing the mineral paragenesis of the Açdif microgabbro (PLA); (**B**,**D**,**E**) Clinopyroxenes grains in microgabbro (PLA); (**C**,**F**) show the development of chlorite on plagioclase (PLA). Cpx: clinopyroxene; Pl: plagioclase; Chl: chlorite.

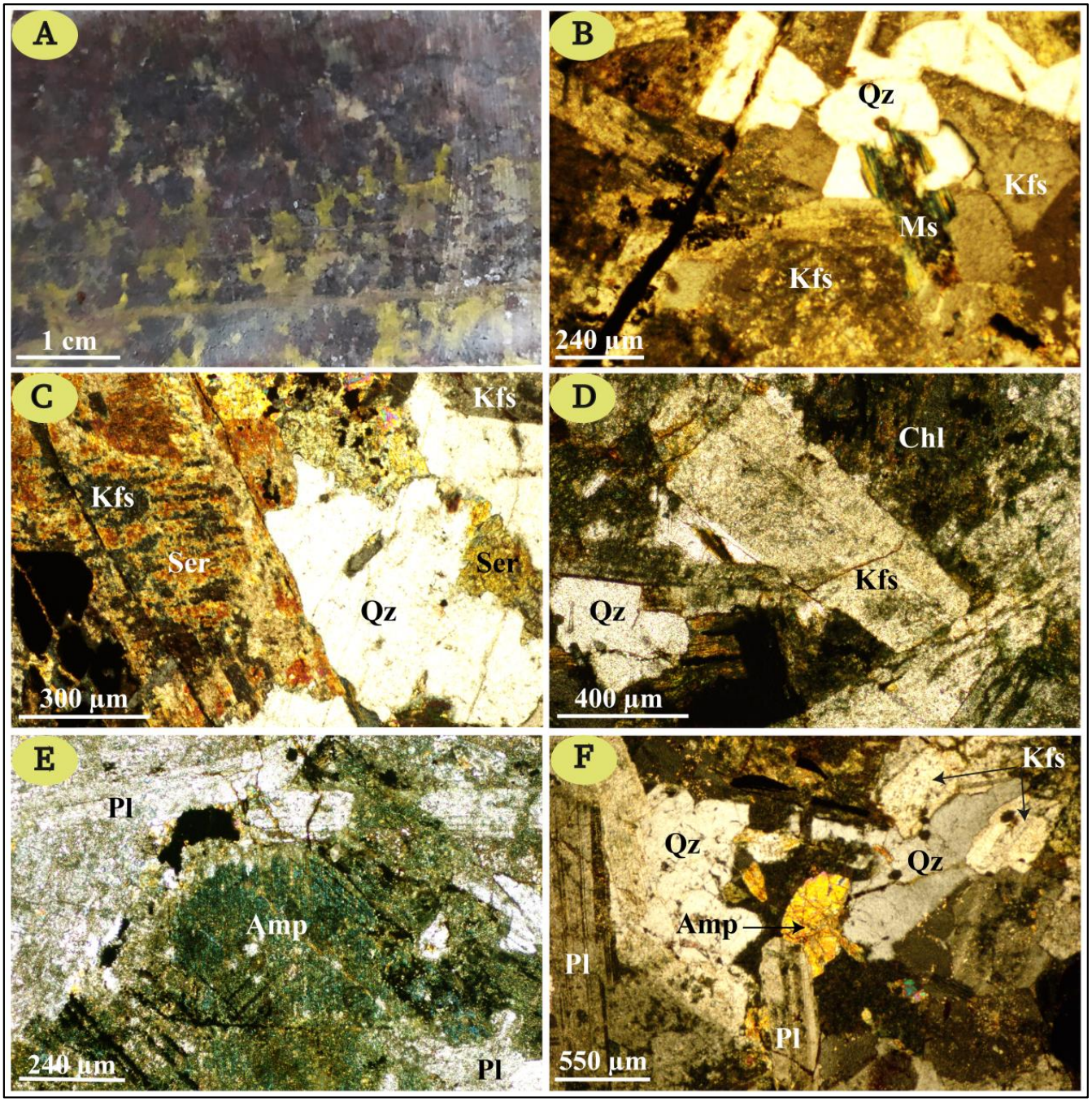


Figure 7. (**A**) Photograph of the quartz diorite in hand specimen; (**B**–**F**) Microphotographs showing the quartz diorite and its mineral paragenesis; (**B**–**D**) mineral paragenesis of quartz diorite. (**C**,**E**) show the alteration of plagioclase and amphibole to sericite (PLA). Pl: plagioclase; Qz: quartz; Kfs: K-Feldspar; Ser: sericite; Amp: amphibole; Chl: chlorite.

4.2. Tectonic

At the scale of the Açdif mine, structural and microstructural analyses carried out during geological mapping works, core drilling surveys, and microscopic observations, have facilitated the identification of several events of ductile and brittle deformations. Chronologically, a penetrative flow schistosity (S1) (Figure 9A,B) affecting the mica-schist base is generally distinguished. It has a direction of N 65° to N 85° with strong dips of the order of 65° to 80° with NW vergence and often parallel to the stratification (S0), which is characterized by quartz-feldspathic layers of centimeter thickness (Figure 9B). Under the

microscope, it is marked by the crystallization of fine flakes of white micas, sericite, and chlorite (Figure 9F). A fracture schistosity (S2) trending N 15° to N 180° with a subvertical dip of approximately 70° to 85° E. This phase also affects the late-formed white milky quartz structures in the area (Figure 3).

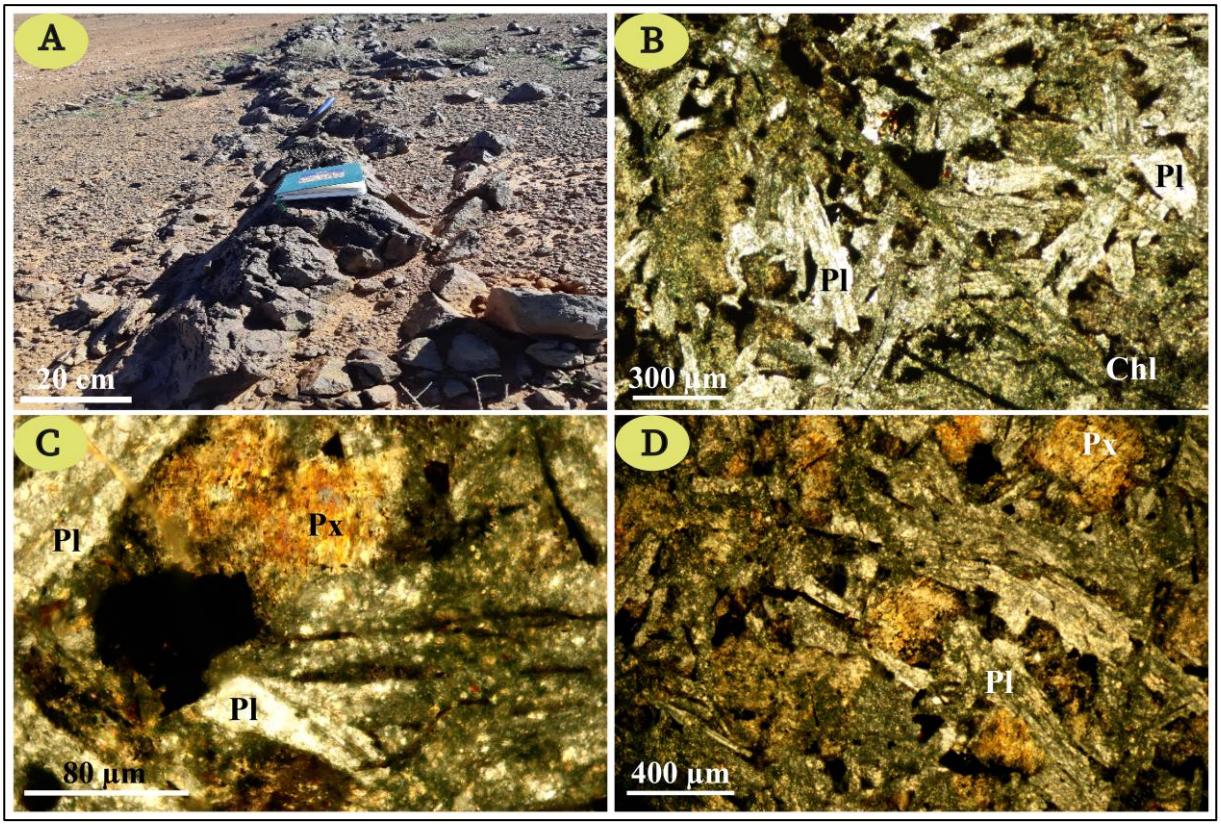


Figure 8. Photos showing the mineral paragenesis of dolerite: (**A**) macroscopic aspect of dolerite; (**B**–**D**) Mineral paragenesis of dolerite facies ((**B**) PLNA; (**C**,**D**) PLA). Px: pyroxene; Pl: plagioclase; Chl: chlorite.

The two schistosity phases (S1 and S2), which correspond to phases D1 and D2, respectively, are consistent with those of the Eburnean orogeny previously described by [19] and [4] in the Zenaga inlier.

Subsequently, the sector was affected by Pan-African events, giving rise to the installation of mafic rock dykes (dolerites and microgabbros) and the development of shear zones. This phase corresponds to the Pan-African phase D1 described in [19]. At the level of the mining quarry of the Açdif deposit, the shear zone is materialized by a corridor of kilometer extension, metric thickness, global direction N 75° to N 80°, and strong dip, 75° N. The fault planes bear tectoglyphs indicating dextral strike-slip kinematics (Figure 9E,J). The intensity of the deformation affecting the schisto-gneissic base increases more and more towards the core of the shear area, giving rise to a strong mylonitization of the encasing rocks (Figure 9G). The area is also punctuated by milky quartz structures and mafic dykes (Figure 1).

In addition, the microscopic analysis of the mineralized corridor reveals various deformation structures and microstructures, indicating ductile and shear deformation. These structures include pressure shadows (Figure 9I), mylonites or tectonites, and tension gashes formed by crack-seal mechanisms (Figure 9C,H). Most of quartz are boudinaged along veins and aligned with the S1 schistosity direction (Figure 9K). This boudinaged quartz is a good kinematic indicator of the shear zone related to the compressive movements of the Pan-African phase (D2).

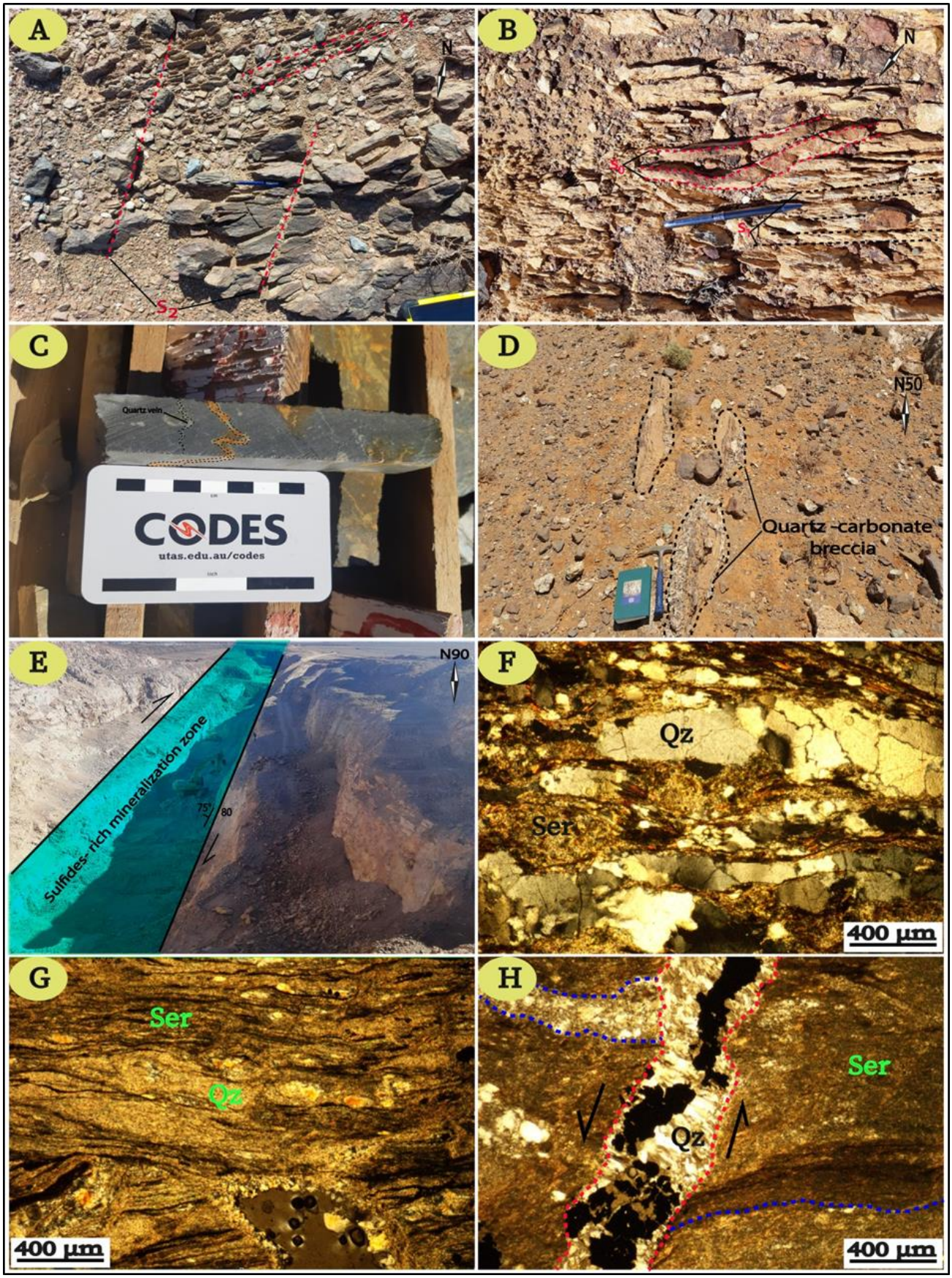


Figure 9. *Cont.*



Figure 9. Illustrations of Eburnean and Pan-African tectonic structures: (**A**) S1 and S2 schistosity developed in metamorphic formations of Paleoproterozoic age. (**B**) S0 layering and (S1) schistosity developed in metamorphic formations of Paleoproterozoic age. (**C**) Mylonite with folded quartz veins. (**D**) Boudinaged quartz veins. (**E**) Edge faults bounding the shear zone. (**F**) S1 schistosity affecting metamorphic rocks. (**G**) Microscopic appearance of mylonite with boudinage. (**H**) Filling of veins with crack-seal (quartz crystals are deformed in the vicinity of the vein walls). (**I**) Microscopic aspect of boudinaged with recrystallized quartz in pressure shadows. (**J**) Fault plane step of pullout. (**K**) Boudinaged quartz veins. Qz: quartz; Ser: sericite; Chl: chlorite.

As for brittle deformation, it results in areas of quartz and carbonate veins and late faults that locally affect the main shear area (Figure 9D). These fractures and faults are likely associated with the late Pan-African phase and may have caused in situ remobilization of mineralization, resulting in precipitation and gold enrichment.

4.3. Geochemistry

In order to supplement the field data and the results of the petrographic study, a geochemical study was carried out using the major elements, trace elements, and rare earth elements. The results of the geochemical analysis are presented in Tables 1 and 2 below.

Table 1. Geochemical analyses of Açdif basic dykes.

Sample	1819 E4	2107 E4	2107 E6	TZL 05-01	TZL 05-02	TZL 0502 A	1819 E6	2107 E5	1819 E7
Facies	**Dolerite**					**Microgabbro**		**Quartz Diorite**	
					(%)				
SiO_2	46.4	50.3	47.8	49.3	50.7	48.7	51.1	50.9	50.3
TiO_2	2.39	2.13	1.65	1.29	2.38	1.64	1.68	1.69	1.82
Al_2O_3	12.9	13.4	14.4	14.6	14.3	14.4	13.2	13.7	15.2
Fe_2O_3	9.31	7.47	10.16	10.31	13.15	9.72	8.35	5.74	7.95
FeO	7.56	7.4	6.36	4.28	2.28	4	5.52	7.96	6.48
MnO	0.26	0.26	0.22	0.24	0.28	0.25	0.28	0.26	0.33
MgO	5.04	6.3	6.41	6.34	3.5	6.56	5.36	6.32	6.06
CaO	9.23	4.16	3.55	6.82	6.34	6.42	6.56	4.27	2.38
Na_2O	1.32	3.15	2.67	2.39	2.3	3.93	2.25	3.67	3.14
K_2O	0.13	0.52	0.7	0.39	0.8	0.27	0.14	0.34	0.18
P_2O5	0.31	0.62	0.16	0.28	0.39	0.24	0.57	0.41	0.37
LOI	5.24	4.62	5.87	3.76	3.55	4.04	5.15	5.06	5.14
Total	100.09	100.33	99.95	100	99.97	100.17	100.16	100.32	99.35
					(ppm)				
Sc	39.00	34.42	40.47	42.06	37.67	36.80	35.37	36.63	39.09
V	462.24	381.51	345.60	319.66	376.79	334.99	319.07	262.23	352.80
Cr	84.00	69.85	131.12	207.60	56.63	242.95	47.22	120.76	82.50
Co	41.38	14.60	47.08	49.02	42.87	51.20	53.29	50.16	57.66
Ni	71.56	62.98	93.22	105.79	51.98	101.22	51.28	74.87	74.78
Cu	104.27	61.58	12.01	77.40	13.10	157.39	189.36	37.17	33.27
Zn	377.75	297.09	258.56	296.54	240.55	196.20	371.65	281.08	409.18
Ga	25.53	23.01	21.07	20.84	28.86	20.53	27.06	21.65	24.94
Rb	15.18	13.73	31.90	13.58	15.41	10.70	8.42	11.39	7.14
Sr	452.29	74.47	100.93	316.78	695.33	266.77	379.68	120.70	173.69
Y	42.92	47.22	27.63	32.95	54.13	29.55	58.47	45.15	40.75
Zr	309.44	324.30	114.09	108.06	343.74	141.89	263.64	270.02	219.12
Nb	18.20	12.48	8.42	5.93	22.09	8.84	16.45	12.58	10.18
Sn	4.15	2.22	1.49	1.95	3.48	1.60	4.01	2.23	2.21
Cs	0.25	0.40	0.78	0.69	0.35	0.60	0.35	0.44	0.34
Ba	59.29	214.75	197.03	261.20	366.52	108.60	70.40	206.49	100.88
La	18.86	22.38	8.68	11.17	23.87	10.49	29.23	21.11	17.34
Ce	45.91	55.74	22.45	26.25	64.03	27.97	74.01	53.54	44.14
Pr	6.21	7.83	3.21	3.78	8.22	4.00	9.96	7.17	6.07
Nd	29.09	36.68	15.29	18.16	37.64	19.04	45.83	34.07	27.81
Sm	8.38	9.64	4.39	5.18	10.35	5.77	12.46	8.95	8.07
Eu	2.09	2.22	1.38	1.52	3.74	1.55	3.44	2.24	2.10
Gd	8.43	9.62	4.75	5.58	10.48	5.99	12.81	9.65	8.04
Tb	1.30	1.52	0.79	0.93	1.64	0.96	1.88	1.43	1.29
Dy	7.90	8.96	4.94	5.75	9.80	5.52	11.51	8.81	7.35
Ho	1.61	1.75	1.01	1.20	1.93	1.11	2.28	1.78	1.46
Er	4.49	4.80	2.79	3.31	5.35	3.10	6.10	4.72	4.15
Tm	0.65	0.71	0.42	0.46	0.80	0.43	0.86	0.71	0.61
Yb	3.83	4.27	2.60	2.89	4.75	2.71	4.80	4.44	3.48
Lu	0.55	0.59	0.38	0.42	0.68	0.40	0.68	0.64	0.48
Hf	7.42	8.12	2.77	2.92	8.03	3.65	6.95	6.82	5.51
Ta	0.86	0.77	0.30	0.35	1.35	0.31	0.89	0.80	0.54
W	0.73	1.03	1.39	0.14	0.47	0.43	0.50	0.36	0.71
Pb	15.36	7.29	7.18	15.00	15.00	13.87	10.15	6.42	7.96
Th	2.56	2.92	0.72	0.88	3.43	0.94	3.24	2.46	2.036
U	1.07	0.85	0.24	0.33	1.07	0.33	0.94	0.81	0.57

Table 2. Geochemical analyses of Açdif granodiorite (bdl: below the detection limit).

Sample	TZL76	TZL77	TZL78	TZL79	TZL80	TZL81	TZL82	TZL83	TZL84	TZL85	TZL86	TZL87	TZL88	TZL89	TZL90
Facies	**Granodiorite**														
	(%)														
SiO_2	70.73	69.2	69.1	65.57	65.73	70.76	70.36	60.84	62.74	68.17	65.14	71.25	63.68	65.87	64.4
TiO_2	0.53	0.5	0.48	0.47	0.46	0.41	0.42	0.46	0.47	0.36	0.44	0.48	0.44	0.34	0.35
Al_2O_3	14.66	16.42	19.83	19.05	20.73	19.47	19.37	17.62	18.3	17.44	18.31	19.53	17.48	17.57	16.22
Fe_2O_3	4.08	4.54	3.22	3.15	2.79	2.27	2.23	2.89	2.94	3.91	3.13	2.76	2.47	2.01	5.02
FeO	4.96	4.96	3.96	3.96	2.96	2.96	2.96	2.96	2.96	3.96	3.96	2.96	2.96	2.96	2.96
MnO	0.03	0.02	0.01	0.01	0.01	bdl	0.01	bdl	bdl	0.02	0.04	bdl	bdl	0.01	0.01
MgO	1.55	1.52	0.82	0.94	1	0.7	0.62	0.69	0.66	1	0.87	0.7	0.72	0.57	0.76
CaO	0.69	0.15	bdl	bdl	bdl	bdl	bdl	bdl	bdl	0.33	2.12	bdl	bdl	0.24	bdl
Na_2O	1.46	1.42	2.01	2.61	3.08	2.83	2.76	2.34	2.06	2.29	2.02	3.84	3.54	2.94	1.06
K_2O	3.93	3.15	3.66	3.64	4.59	3.51	2.89	3.93	3.93	2.72	3.69	2.94	2.59	3.14	4.62
P_2O_5	0.05	0.05	0.07	0.07	0.09	0.06	0.06	0.07	0.07	0.05	0.08	0.08	0.07	0.07	0.05
LOI	2.25	1.79	0.90	1.03	1.1	0.77	0.682	0.759	0.73	1.36	2.62	0.77	0.79	0.81	0.84
Total	99.96	98.76	100.10	96.54	99.58	100.78	99.40	89.60	91.90	97.65	98.46	102.35	91.78	93.57	93.33
	(ppm)														
Sc	5.21	12.23	7.16	4.96	4.00	4.42	4.01	4.23	4.14	3.30	7.70	4.75	4.58	3.31	4.62
V	109.71	109.71	109.71	109.71	109.71	109.71	109.71	109.7	109.71	109.71	109.71	109.71	109.71	109.71	109.71
Cr	135.00	175.00	146.00	217.00	187.00	111.00	164.00	91.00	125.00	128.00	106.00	105.00	103.00	257.00	116.00
Co	143.00	bdl	bdl	bdl	bdl	bdl	bdl	49.00	bdl	76.00	bdl	bdl	bdl	bdl	14.00
Ni	88.00	39.00	41.00	52.00	39.00	30.00	47.00	51.00	35.00	42.00	33.00	42.00	39.00	30.00	54.00
Cu	56.00	50.00	25.00	26.00	18.00	23.00	69.00	29.00	15.00	23.00	62.00	30.00	27.00	14.00	25.00
Zn	61.00	33.00	bdl	29.00	2.00	6.00	20.00	bdl	bdl	10.00	bdl	bdl	bdl	bdl	17.00
Ga	26.03	26.03	26.03	26.03	26.03	26.03	26.03	26.03	26.03	26.03	26.03	26.03	26.03	26.03	26.03
Rb	151.33	150.33	153.33	149.33	143.33	151.33	150.33	152.33	154.33	152.33	151.33	150.33	155.33	152.33	154.33
Sr	60.00	58.00	87.00	90.00	91.00	92.00	99.00	77.00	69.00	75.00	54.00	94.00	92.00	92.00	49.00
Y	6.00	11.00	5.00	5.00	bdl	2.00	2.00	2.00	2.00	3.00	4.00	bdl	bdl	2.00	4.00
Zr	25.10	26.60	23.00	19.70	31.10	39.90	17.30	43.40	21.40	20.80	27.40	33.80	28.70	15.90	36.50
Nb	10.00	10.00	9.00	10.00	11.00	10.00	10.00	9.00	10.00	10.00	10.00	10.00	11.00	10.00	10.00
Sn	40.00	65.00	44.00	56.00	21.00	53.00	59.00	39.00	55.00	45.00	bdl	55.00	22.00	45.00	26.00
Cs	2.73	2.73	2.73	2.73	2.73	2.73	2.73	2.73	2.73	2.73	2.73	2.73	2.73	2.73	2.73
Ba	957.00	550.00	536.00	520.00	615.00	656.00	1258.00	1027.00	980.00	1115.00	495.00	380.00	467.00	749.00	749.00
La	51.28	33.68	45.40	70.60	59.85	55.84	57.76	48.12	52.84	45.46	45.54	34.14	34.06	45.65	50.71
Ce	115.00	73.68	97.67	148.40	129.20	113.90	124.00	102.70	113.30	92.84	104.30	78.51	77.75	93.56	106.20
Pr	12.67	8.07	11.51	16.31	14.00	13.24	14.84	11.62	13.34	10.51	11.71	8.84	8.67	9.76	11.36
Nd	52.79	32.45	42.02	60.49	56.99	52.16	53.32	44.82	51.60	38.46	48.72	36.41	35.64	37.77	45.02
Sm	9.53	7.49	7.68	11.30	8.82	7.29	7.78	10.44	9.36	8.40	10.16	7.28	7.10	6.53	8.49
Eu	1.17	0.99	1.14	1.64	1.34	1.16	1.32	1.41	1.57	1.06	2.11	1.32	1.33	0.99	1.29
Gd	6.41	6.40	6.97	6.50	5.38	4.40	4.87	5.70	7.10	4.69	7.74	5.06	4.95	4.72	6.18
Tb	0.49	0.43	0.41	0.45	0.38	0.30	0.34	0.41	0.43	0.35	0.64	0.35	0.34	0.35	0.49
Dy	1.35	1.60	1.34	1.31	1.05	0.78	0.97	1.08	1.13	1.01	2.16	0.88	0.84	1.01	1.45
Ho	0.20	0.27	0.22	0.21	0.16	0.11	0.16	0.15	0.45	0.15	0.37	0.11	0.11	0.15	0.19
Er	0.57	0.75	0.63	0.69	0.53	0.37	1.46	0.46	1.39	0.43	1.11	0.36	0.34	0.42	0.51
Tm	0.07	0.09	0.07	0.17	0.05	0.03	0.05	0.05	0.05	0.05	0.26	0.04	0.04	0.04	0.05
Yb	0.43	0.63	0.52	0.49	0.32	0.19	0.39	0.31	0.31	0.30	0.99	0.27	0.26	0.26	0.29
Lu	0.08	0.10	0.08	0.07	0.05	0.03	0.05	0.05	0.05	0.04	0.15	0.04	0.04	0.04	0.04
Hf	9.77	9.37	9.17	8.97	9.07	9.87	9.17	8.77	10.00	8.92	9.06	9.77	9.47	8.87	9.78
Ta	0.64	0.44	0.54	0.59	0.57	0.56	0.61	0.49	0.46	0.51	0.49	0.47	0.53	0.57	0.52
W	bdl	bdl	bdl	bdl	bdl	bdl	bdl	bdl	bdl	bdl	bdl	bdl	bdl	bdl	bdl
Pb	64.00	34.00	bdl	37.00	bdl	bdl	bdl	bdl	bdl	bdl	bdl	bdl	bdl	bdl	43.00

4.3.1. Major Elements and Traces

The chemical composition of the magmatic rocks in the Açdif sector show two large sets, E1 and E2:

- Mafic and intermediate rocks (together, E1) are represented by dolerites, microgabbro and quartz diorite. They show variable levels of SiO_2 (46.4–57.6 wt%), TiO_2 (0.54–2.39 wt%), K_2O (0.31–3.93 wt%), and Na_2O (0.26–9.23 wt%).
- Felsic rocks (together, E2) are represented by granodiorite with SiO_2 contents (63.68–70.76 wt%), TiO_2 (0.34–0.53 wt%), K_2O (2.72–4.62 wt%), and Na_2O (1.06–3.84 wt%). The plots of the chemical analyses in the TAS diagrams [23,24], and Zr/TiO_2—Nb/Y diagram [25] show two sets (E1 and E2) with a variety of compositions ranging from basalt, including diorite, and gabbro-diorite (Figure 10). As for the E2 set, it occupies the field of granodiorites and confirms petrographic observations (Figure 10A–D). The dykes of the E1 set are characterized by average silica values ranging from 46.40 to 57.60 wt% from microgabbro-dolerite to diorite. MgO contents are low and slightly decrease from microgabbro (6.56 wt%) to quartz diorite (6.06 wt%). The Mg* ratio varies from 41 for microgabbro-dolerite to 33 for quartz diorite. These low values are accompanied by a fall in the contents of elements in transition traces, especially chromium and nickel (Figure 11). The low ratios in Mg* have the characteristics of

magmas that have evolved by fractional crystallization [26]. CaO gradually decreases from microgabbro-dolerites (6.12 wt%) to quartz diorite (3.32 wt%). This decrease is accompanied by an increase in Na_2O (3.40 wt%) levels. MnO contents are low, but significant. They are relatively lower in microgabbro and dolerite (0.25 wt%) and higher in microgabbro-dolerites by reaching the maximum values (0.30 wt%) in diorite. The increase in Fe_2O_3, TiO_2, Zr, Hf, Sr, and Th with the decrease in MgO in these facies may be compatible with early fractionation of plagioclase and pyroxene compared to other mineral phases. This membership is confirmed by the increase in Fe_2O_3 and TiO_2 contents during differentiation (Figure 11). The early crystallizations of plagioclases and pyroxenes compared to ferro-titaniferous oxides and quartz are typical of rocks in the tholeiitic series.

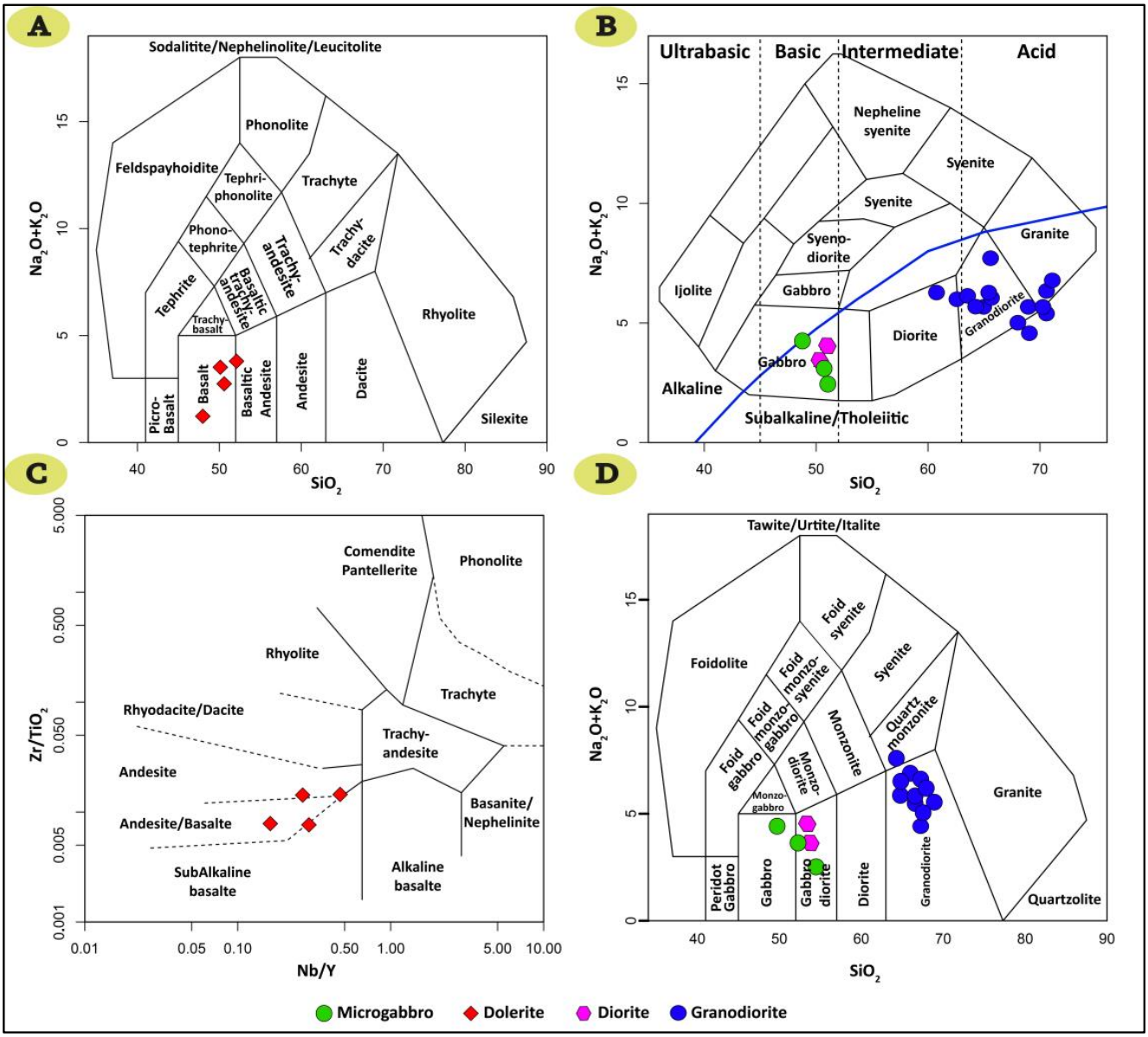


Figure 10. Projection of Açdif rocks classification diagrams: (**A**) SiO_2 − Na_2O + K_2O, TAS [23]; (**C**) Zr/TiO_2Nb/Y [25] "Volcanic rocks", TAS diagrams; (**B**,**D**) SiO_2 − Na_2O + K_2O [24] "Plutonic rocks".

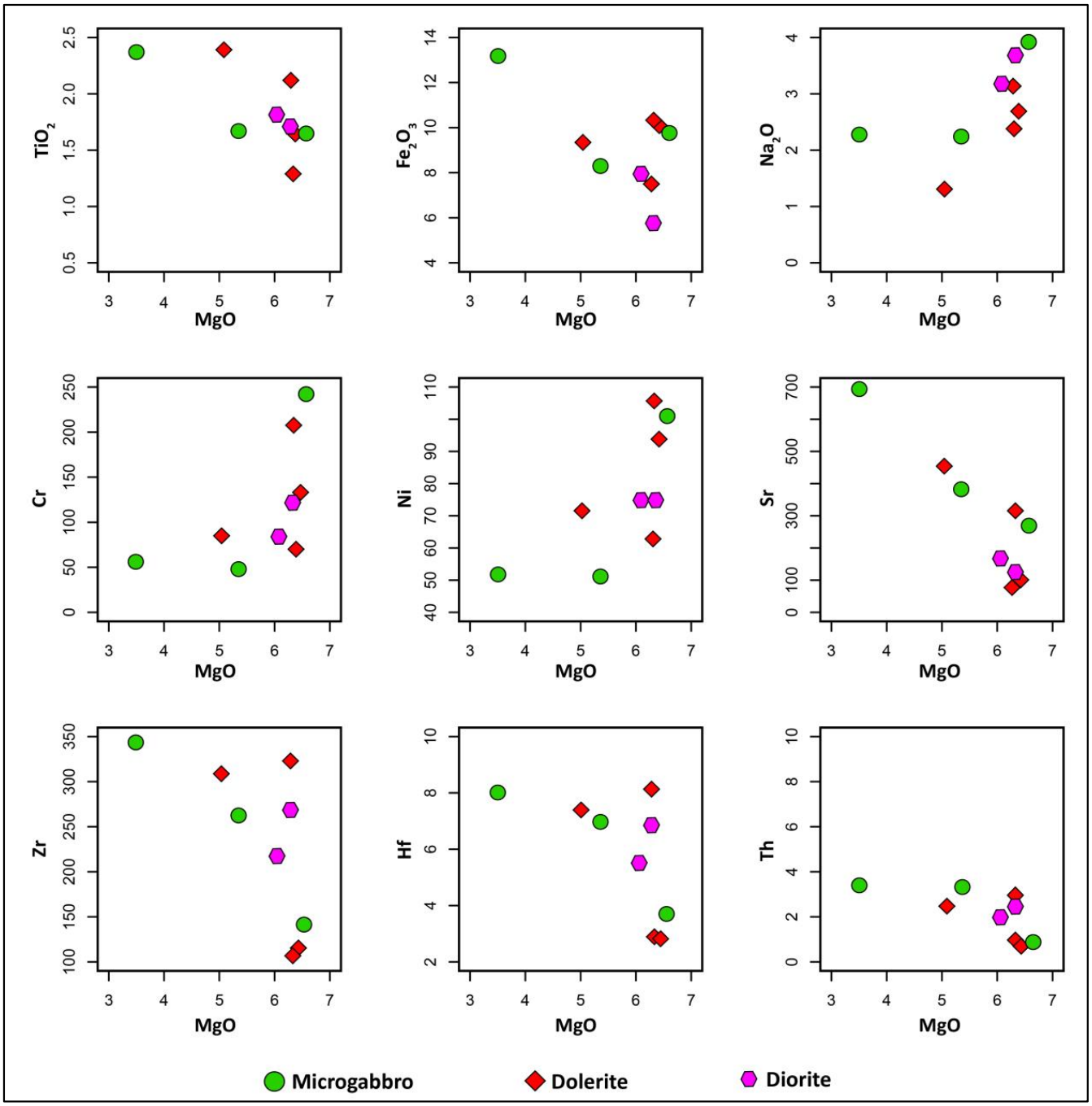


Figure 11. Major element (wt%) and trace element (ppm) versus MgO (wt%) in basic dykes (Microgabbro, dolerite, and diorite) [27].

In the chemical affinity diagrams K_2O vs. SiO_2 of [28] and the AFM diagram [29], (Figure 12A,B), two entities with different characters are distinguished; the first set corresponds to the Azguemerzi granodiorite, which is typically calc-alkaline to highly potassium calc-alkaline. This position of the second set in the tholeiitic field corresponds to the mafic dykes of Açdif (microgabbro, dolerite, and quartz-diorite) (Figure 12A,B). The application of geochemical diagrams such as the La/10–Y/15–Nb/8 diagram [30] and the Zr-Ti diagram [31,32] to the magmatic formations of Açdif shows that mafic dykes are part of the field of the basalts from the intraplate context [8] and in a distensive orogenic context (Figure 13A–C), while Azguemerzi granodiorites occupy the arc granite field in a syn-collisional compression context (Figure 13A,D,E).

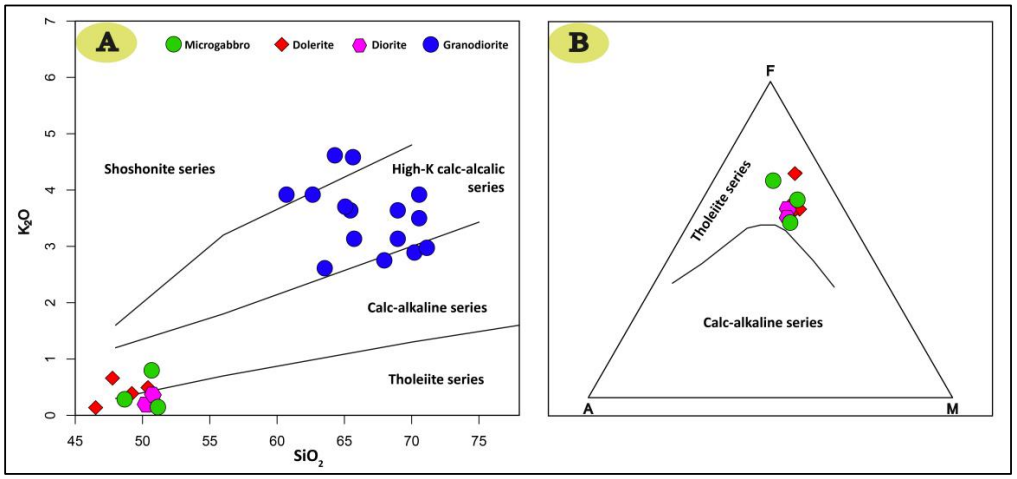


Figure 12. Projection of the magmatic rocks of Açdif in the (**A**) K_2O vs. SiO_2 diagram [28] and in the (**B**) AFM diagram [29].

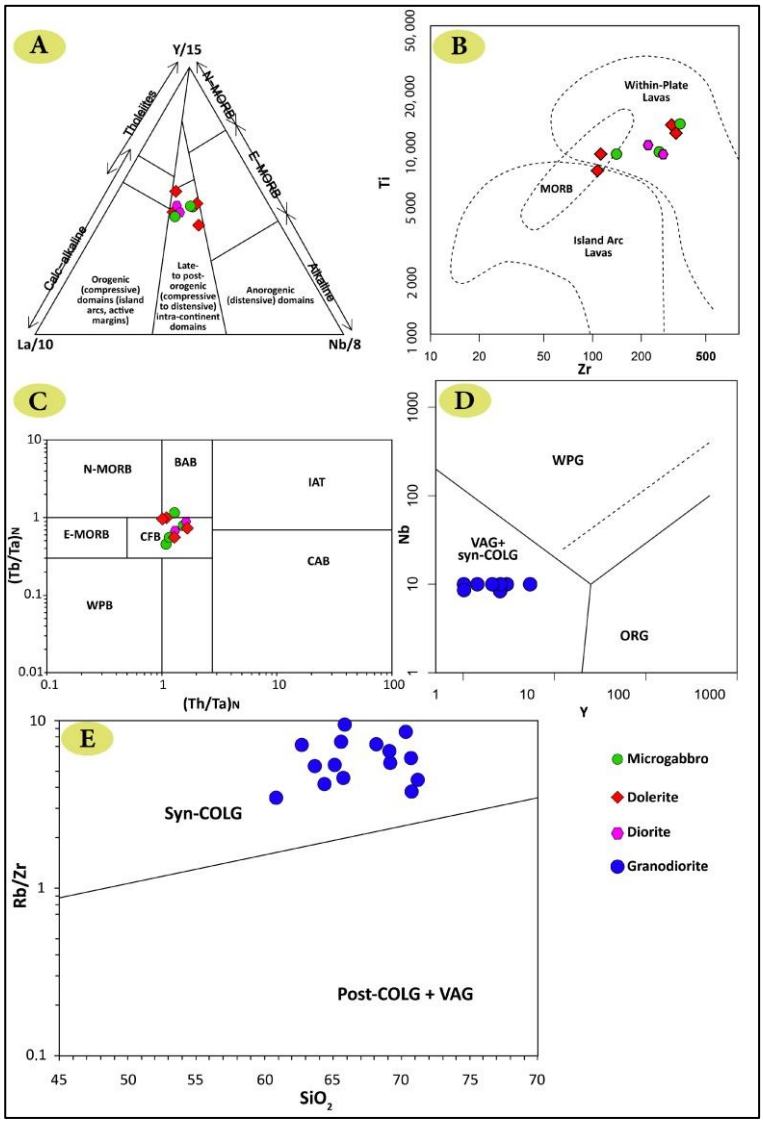


Figure 13. Discrimination diagram of geotectonic sites: (**A**) La/10–Y/15–Nb/8 ternary classification diagram [30]; (**B**) Zr-Ti diagram [31]; (**C**) $(Th/Ta)_N$-$(Tb/Ta)_N$ plot [33] for the Açdif dykes; (**D**) Y-Nb diagram [34]; (**E**) SiO_2-Rb/Zr diagram.

4.3.2. REE

For the dykes of Açdif, the appearance of the spectra of rare earth normalized with respect to the primitive mantle [34] (Figure 14A), as well as the values of the ratio (La/Yb), are identical to those of most continental tholeiites [33,35,36]. This rock group shows high levels of light rare earth with relatively high ratios: (La/Yb) = 3.34–6.08, and (La/Sm) = 1.81–2.40. Multi-elementary diagrams (Figure 14B), where the elements are standardized against chondrites [37], are used in discriminating the geodynamic sites for emplacement of the different tholeiitic series. They clearly highlight the continental tholeiitic character of these rocks (Nb/Y values less than 0.70 (0.26–0.42)) [38]. The spectra of the different facies (microgabbro, dolerite, and diorite) are similar and suggest a common source of their magmas. Like most continental tholeiites, these are characterized by an enrichment with highly incompatible elements (LILE) Rb, Ba, K, Th, and light rare earth, as well as a slight negative anomaly in Nb and an overall negative slope of the spectrum.

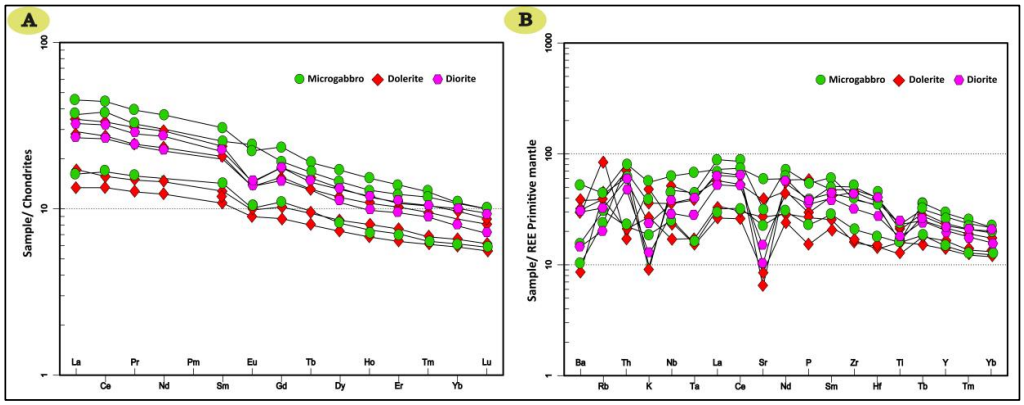


Figure 14. (**A**) Diagrams of rare-earth spectra normalized to the early mantle [34] and (**B**) multi-element diagram normalized to chondrites [39] for the Açdif dykes.

The spectra of the rare earth of Azguemerzi granodiorite (Figure 15A) are characterized by a less-pronounced Eu anomaly (Eu*/Eu: 0.44 to 0.73, with higher overall rare earth levels (ΣREE: 166.6–318.6). They are more enriched in LREE (LaN: 109.87–227.7) and more split with (LaN/LuN: 36.7 to 106.07). HREE show flatter spectra (DyN/LuN: 1.46–3.46). The multi-elementary distribution (rare earth and some major elements) has been reported in spider diagrams standardized with respect to the ORGs (oceanic rift granite) [32]. Azguemerzi granodiorite shows a distribution of elements comparable to those of calc-alkaline rocks [20], with more pronounced negative anomalies in Zr (Figure 15B).

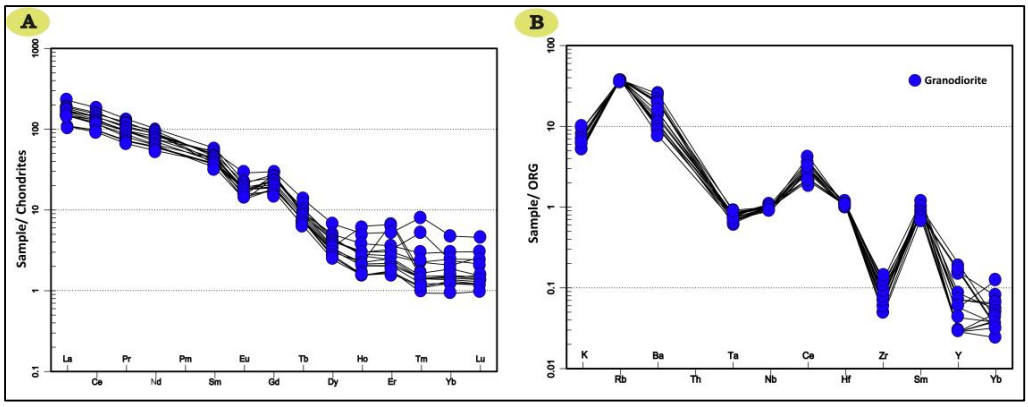


Figure 15. (**A**) Diagrams of rare-earth spectra normalized to chondrite [40] and (**B**) multi-element diagram normalized to ORG [32] for granodiorite.

5. Discussion and Interpretation

5.1. Structural Control

All the formations outcropping in the Açdif sector have undergone several tectonic events that have affected the Anti-Atlas region. These events result in ductile and brittle deformations.

However, the old deformation events in the sector are represented by a penetrative S1 schistosity of global direction N65 to N70 parallel to the S0 stratification. The orthogneissification of the Azguemerzi granodiorites may also be linked to this ancient event [19]. This deformation of the Paleoproterozoic base belongs to the Eburnean orogenic event [4].

The structures of the Pan-African orogeny are materialized by the following: (i) Basic dykes emplaced along two major trending directions: NE-SW and NW-SE.This event is linked to an extension of the passive margin of West African [8,14] and the opening of an oceanic basin in the BouAzzer inlier [41,42] and in the Siroua inlier [43–45]. (ii) The development of the dextral shear zone of Açdif, from global direction of ENE-WSW with a dip of 75° to the north. This area carries most of the gold mineralization of the deposit, in the form of inclusion in pyrite in dissemination in deformed gneissic rock or in quartz veins. The paroxysm of the deformation on this suture is marked by the development of the C/S factories, by a mylonitization of the encasing rock and the pudding areas in the quartz veins that punctuate the shear zone. The pudding shape is probably due to subsequent compressive events.

The late events of deformation are marked by an extensive brittle episode that results in areas of quartz and carbonate breaches. This phase can cause remobilization of mineralization, which is accompanied by precipitation and gold enrichment.

5.2. Geochemical Constraints

The geochemical data of the Açdif dykes show several criteria that are similar to those of the MORB: $CaO/TiO_2 < 17$ and $Al_2O_3/TiO_2 < 20$ [46,47], with high titanium contents corresponding to CaO/TiO_2 (0.48) and Al_2O_3/Ti. The levels obtained in zirconium (108.06 to 343.74 ppm) and vanadium (109.70 to 462.23 ppm) are also comparable to those of P-MORB-type basalts and are significantly higher than those of arc tholeiites [47,48]. The ratios Gd/Yb and La/Sm vary, respectively, from 1.82 to 2.30 and 1.81 to 2.35 and fall within the range of basalt values of the different MORBs [47,49]. The different types of MORB are discriminated against according to their content of incompatible trace elements. Therefore, the Zr/Nb, Zr/Y, and Y/Nb ratios are very significant indicators of the impoverished or enriched nature of the generating mantle [47]. The dykes of Açdif have ratios Zr/Y (3.27 to 12.77), Zr/Nb (13.55 to 33.24), Y/Nb (2.35 to 5.55), and Ti/Zr (9.85 to 86.77). The comparison between these values shows that there is a great similarity between these dykes and those that characterize the MORB (Zr/Y (3.9 to 7.9) and Ti/Zr (64 to 84) [48–52]. Chemical analyses of Azguemerzi granodiorite generally confirm their intermediate character (Table 2). It is enriched with alkaline elements and is characterized by fairly moderate levels of SiO_2 (57.60 to 71.27 wt%); the levels of Fe_2O_3, MgO, and TiO_2 depend on the abundance of colored minerals and plagioclase.

5.3. Geodynamic Context

Açdif granodiorite is part of the Azguemerzi granitic intrusions of Paleoproterozoic age (U-Pb on zircon/2032 ± 5 Ma) and Tazenakht monzogranite (U-Pb on zircon/2037 ± 9 Ma) [5]. These granitoids are comparable to those of the Ighrem inlier (U–Pb zircon/2050 ± 6 Ma) [53], the Tagragra inlier of Tata (U–Pb SIMS/2046 ± 8 Ma) (Walsh et al. 2002) [54], the Akka Tagragra inlier (Pb–2004), the Low Drâa inlier (U–Pb/2037 ± 37 Ma) [55], and the Sirwa inlier (U–Pb SIMS/2045 ± 10 Ma) [5,56]. These granitoids were affected by a low-grade ductile deformation during Pan-African tectono-metamorphic events that mainly affect Tazenakht granite, in a more northern position. They have been attached to a post-collisional context because they are of calc-alkaline affinity rich in biotite [57], while Tazenakht leucogranites are syn-collisional [58,59]. The calc-alkaline character of Azguemerzi granitoids is also argued by several geological works [8–10,14]. These granitoids are earlier than the swarms

of dykes and sills of doleritic to gabbroic mafic rocks nature known as the Ifzwane suite [10]. In the Açdif sector, these dykes show a variety of facies ranging from microgabbro and dolerite to quartz diorites. They also show several directions N-S to NW-SE and NE-SW to E-W. These mafic dykes are also comparable to those of the mafic sills and dykes described in other inliers of the western Anti-Atlas (Bas-Drâa, Kerdous, Agadir Melloul, and Iguerda Taïfast inliers). They have a series of ages ranging from 2040 ± 2 Ma to 885 ± 28 Ma. The authors of [6] suggested that granitic liquids were generated by a partial fusion of the lower crust relating to the production of basaltic magma, perhaps in relation to a mantellic plume of 2040 Ma and a bimodal magmatic event of 2040 Ma. The dykes attributed to this age of 2040 Ma, could correspond to the first magmatic event related to an extensive phase at the Anti-Atlas scale. The bimodal character with continental tholeiitic affinity of mafic dykes has been confirmed by several studies and could be linked to the Pan-African distensive tectonic phase that affected the Zenaga inlier and the West African cardboard [8,15–18].

5.4. Characterization of the Source

Generally, enrichment with LILE and light rare earths is among the characteristics of continental tholeiites. It is interpreted as the effect of a crustal contamination process [35,60,61]. In the case of the continental tholeiites of Açdif, the ratios of incompatible elements are in favor of their derivation from an enriched source such as those of enriched MORBs (P-MORB). Indeed, the ratios Zr/Y (~6.12), Zr/Nb (~19.86), (La/Ce) N < (1), and Ti/Zr (~49.05) indicate an enriched origin [48–52]. The role of crustal contamination is also suggested by (i) the high values of the Th/Ta ratio (2.77 on average) generally observed in continental tholeiites, and signs of crustal contributions [62]; (ii) the relatively high values of the Ba/Zr ratio (0.46–2.41), which, according to [63], would be due to crustal contamination; and (iii) the values of the Nb/U ratio (14.62–26.85), which, according to [64], suggest the intervention of a crustal component. Rocks derived from the mantle, such as OIBs and MORBs, have a Nb/U ratio of 47 ± 10 [65]. The values in this ratio are 21 and 9, respectively, for the lower crust and the upper crust [66]. Thus, basalts derived from the mantle and contaminated by the crust have Nb/U ratios < 47 ± 10. The analogy of the Açdif mafic dykes with E-MORBs and the intervention of the crustal contamination process were also discussed, for Zenaga doleritic dykes, in [8]. The representative points of the rocks were spread between the E-MORBs and the average of the continental crust. The contamination and crustal intake in the continental tholeiites of Açdif is supported by what has been suggested by [6] to be the age of some mafic Zenaga dykes (2040 Ma) and which corresponds to the age of the Azguemerzi granitoids genetically prior to the latter.

5.5. Age of Implementation

The Açdif area is mainly taken into the magmatic and metamorphic formations of the Eburnean basement. Magmatic rocks are geochemically different. Field observations as well as the petro-geochemical study of the rocks of the E1 set suggest that they were derived from a single magmatic source by fractional crystallization. The geochemical study (major elements, traces, and rare earths) of the mafic dykes of Açdif clearly shows the mineralogical and geochemical characteristics of continental tholeiites. They have a chemical composition closer to that of enriched MORBs (E-MORB). They are comparable to other continental tholeiites in Morocco and located worldwide: Mesozoic and Paleozoic continental tholeiites [33,34,52,67,68], Neoproterozoic continental tholeiites of the Zenaga inlier in the western Anti-Atlas [8,69], and those of the Congo craton linked to the Pan-African stage [36]. This magmatism therefore testifies to an extension phase that has affected this part of the northern border of West African craton [8]. However, geochronological studies carried out at the scale of the inlier, with the exception of the results of the two massifs dating from 2040 ± 2 Ma [6], were able to reveal absolute dates ranging from 1650 Ma to 885 Ma [6,9]. The latter are consistent with the intra-plate magmatic event extended to 1750 Ma, known in the West African craton (WAC) [9]. The age margin (1650 Ma to 885 Ma) could be explained by the process of fractional crystallization of

source magma that has evolved by generating several facies (this study). A similar event is reported in other crustal blocks, including in the northwest of the Laurentian [70] and in Siberia [71], southeast of the Baltic (southern Ural region). The magmatism dated around 1750 Ma is supposed to result from a single event on a global scale [9,72]. This event was probably preceded by a major event more than 2032 ± 5 Ma and 2037 ± 9 Ma ago [5]. This results in a huge amount of magma of which Azguemerzi granodiorite is a part. The geochemical study of this rock clearly shows a highly potassium calc-alkaline and calc-alkaline character linked to a syn- to post-collision orogenic geodynamic context. This aluminous facies (biotite, garnet, and muscovite) and its association with migmatitic rocks suggest that these granitoids come from the partial fusion of the crust. The absolute dates obtained for these granitoids (granodiorite) in the Zenaga inlier (Pb on zircon/2032 ± 5 Ma) (U-Pb on zircon/2037 ± 9 Ma) [5] are probably quite close to the maximum conditions of Eburnean orogeny in this part of the West African craton.

6. Conclusions

The Açdif area is encased in the Paleoproterozoic geological formations of the Zenaga inlier. These trainings are structured according to the Eburnean and Pan-African orogeny. The mapping and petro-geochemical study carried out on Açdif granitoids and mafic dykes, allow us to conclude the following:

(i) The Açdif sector is formed from a set of plutonic magmatic rocks composed mainly of granodiorite (Azguemerzi granitoids) and a set of late mafic dykes (Ifzwane suite) materialized by microgabbros, dolerites, and quartz diorite. These sets of dykes would come from the same magmatic chamber by fractional crystallization process.

(ii) The structural analysis made it possible to distinguish a dextral shear zone evolving from a ductile to brittle regime, with the development of gold mineralization in the deformed host-rocks and which is mainly associated with the iron oxides in the brecciated quartz veins.

(iii) The geochemical data confirm the field observations and the petrographic investigations of the dykes and granodiorites. These latter have calc-alkaline signatures with highly potassium calc-alkaline affinity relating to a geodynamic arc context. On the other hand, mafic dykes show a bimodal character of continental tholeiites comparable to those of E-MORB and linked to a context of distension.

Author Contributions: Conceptualization, M.E.A. and M.A. (Mohamed Aissa); data curation, M.E.A., M.A. (Moussaid Azizi), S.I., M.Z., L.M., S.A. and I.P.; writing—original draft preparation, M.E.A., M.A. (Mohamed Aissa), S.I. and A.M.; writing—review and editing, M.E.A., M.A. (Moussaid Azizi), A.M., S.I. and H.M., H.O. and M.A. (Mohammed Aarab), M.S., I.P. and I.L.; visualization, M.E.A.; supervision, M.A. (Mohamed Aissa); project administration, M.E.A. and M.A. (Moussaid Azizi); funding acquisition, M.E.A. and I.P. All authors have read and agreed to the published version of the manuscript.

Funding: This research received no external funding.

Conflicts of Interest: The authors declare no conflict of interest.

References

1. Bleeker, W. The late Archean record: A puzzle in ca. 35 pieces. *Lithos* **2003**, *71*, 99–134. [CrossRef]
2. Leblanc, M. The late Proterozoic ophiolites of Bou Azzer (Morocco): Evidence for Pan-African plate tectonics. In *Developments in Precambrian Geology*; Elsevier: Amsterdam, The Netherlands, 1981; Volume 4, pp. 435–451.
3. Saquaque, A.; Admou, H.; Cisse, A.; Benyousef, A.; Reuber, I. Les intrusions calco-alcalines de la boutonnière de Bou Azzer-El Graara (Anti-Atlas, Maroc): Marqueurs de la déformation panafricaine majeure dans un contexte de collision d'arc. *C. R. Acad. Sci.* **1989**, *308*, 1279–1283.
4. Choubert, G. *Histoire Géologique du Précambrien de l'Anti-Atlas*; Éditions du Service géologique du Maroc: Rabat, Morocco, 1963.
5. Thomas, R.; Chevallier, L.; Gresse, P.; Harmer, R.; Eglington, B.; Armstrong, R.; De Beer, C.; Martini, J.; De Kock, G.; Macey, P. Precambrian evolution of the Sirwa window, Anti-Atlas orogen, Morocco. *Precambrian Res.* **2002**, *118*, 1–57. [CrossRef]

6. Kouyaté, D.; Söderlund, U.; Youbi, N.; Ernst, R.; Hafid, A.; Ikenne, M.; Soulaimani, A.; Bertrand, H.; Chaham, K.R. U–Pb baddeleyite and zircon ages of 2040 Ma, 1650 Ma and 885 Ma on dolerites in the West African Craton (Anti-Atlas inliers): Possible links to break-up of Precambrian supercontinents. *Lithos* **2013**, *174*, 71–84. [CrossRef]
7. Horrenberger, J.-C. *Tectonique Superposées Dans le Précambrien de Taznakht (Anti-Atlas Central, Maroc)*; 15p+planches+annexes; University Louis Pasteur: Strasbourg, France, 1973.
8. Hafid, A.; Sagon, J.; Julivert, M.; Arboleya, M.; Saquaque, A.; El Boukhari, A.; Saidi, A.; Soler, J. Neoproterozoic basic dykes of the Zenaga Inlier, central Anti-Atlas, Morocco: Petrology, geochemistry and geodynamic significance. *J. Afr. Earth Sci.* **2001**, *32*, 707–721. [CrossRef]
9. Youbi, N.; Kouyaté, D.; Söderlund, U.; Ernst, R.E.; Soulaimani, A.; Hafid, A.; Ikenne, M.; El Bahat, A.; Bertrand, H.; Chaham, K.R. The 1750 Ma magmatic event of the west African craton (Anti-Atlas, Morocco). *Precambrian Res.* **2013**, *236*, 106–123. [CrossRef]
10. Thomas, R.J.; Fekkak, A.; Ennih, N.; Errami, E.; Loughlin, S.; Gresse, P.; Chevallier, L.; Liégeois, J.-P. A new lithostratigraphic framework for the Anti-Atlas Orogen, Morocco. *J. Afr. Earth Sci.* **2004**, *39*, 217–226. [CrossRef]
11. Ikenne, M.; Mortaji, A.; Gasquet, D.; Stussi, J.M. Les filons basiques des boutonnières du Bas Drâa et de la Tagragra d'Akka: Témoins des distensions néoprotérozoïques de l'Anti-Atlas occidental (Maroc). *J. Afr. Earth Sci.* **1997**, *25*, 209–223. [CrossRef]
12. El Bahat, A.; Ikenne, M.; Söderlund, U.; Youbi, N.; Ernst, R.; Soulaimani, A.; El Janati, M.; Hafid, A. U–Pb ages of dolerite dykes in the Bas Drâa Inlier of the Anti-Atlas of Morocco: Newly identified 1380 Ma event in the West African Craton. *Lithos* **2013**, *174*, 85–98. [CrossRef]
13. Hafid, A.; Sagon, J.; Saidi, A. La serie metamorphique du Proterozoique inferieur de la boutonniere d'Irherm (Anti-Atlas Occidental, Maroc): Petrographie, geochimie et apercu structural. *Afr. Geosci. Rev.* **1998**, *5*, 145–150.
14. Hafid, A. *Magmatisme Basique Filonien Néoproterozoïque (Précambrien II Inférieur) dans l'Anti-Atlas Central et Occidental: Minéralogie, Géochimie, Pétrogenèse et Implication Géodynamique*; Faculté des Sciences-Semlalia, Université Cadi Ayyad: Marrakesh, Morocco, 1999.
15. Caby, R. Paleogeodynamique d'une marge passive et d'une marge active au Precambrien superieur; leur collision dans la chaine pan-africaine du Mali. *Bull. Société Géologique Fr.* **1978**, *7*, 857–861. [CrossRef]
16. Black, R.; Caby, R.; Moussine-Pouchkine, A.; Bayer, R.; Bertrand, J.; Boullier, A.; Fabre, J.; Lesquer, A. Evidence for late Precambrian plate tectonics in West Africa. *Nature* **1979**, *278*, 223–227. [CrossRef]
17. Castaing, C.; Feybesse, J.; Thiéblemont, D.; Triboulet, C.; Chevremont, P. Palaeogeographical reconstructions of the Pan-African/Brasiliano orogen: Closure of an oceanic domain or intracontinental convergence between major blocks? *Precambrian Res.* **1994**, *69*, 327–344. [CrossRef]
18. Dupont, P.; Lapierre, H.; Gravelle, M.; Bertrand, J. Caractérisation du magmatisme Protérozoïque supérieur en Afrique de l'ouest et implications géodynamiques: Des rifts intracratoniques au Panafricain? *Can. J. Earth Sci.* **1987**, *24*, 96–109. [CrossRef]
19. Ennih, N.; Liégeois, J.-P. The Moroccan Anti-Atlas: The West African craton passive margin with limited Pan-African activity. Implications for the northern limit of the craton. *Precambrian Res.* **2001**, *112*, 289–302. [CrossRef]
20. Saidi, A. *Pétrographie, Géochimie, et Structure Des Formations Métamorphiques D'âge Paléoprotérozoïque et Des Zones de Cisaillements Ductile au Nord de la Boutonnière de Zenaga (Anti-Atlas, Maroc)*; Université Cadi Ayyad: Marrakech, Morocco, 2002.
21. Gasquet, D.; Ennih, N.; Liégeois, J.-P.; Soulaimani, A.; Michard, A. The pan-african belt. In *Continental Evolution: The Geology of Morocco: Structure, Stratigraphy, Tectonics of the Africa-Atlantic-Mediterranean Triple Junction*; Springer: Berlin/Heidelberg, Germany, 2008; pp. 33–64.
22. Gresse, P.G.; De Beer, C.H.; De Kock, G.S.; Thomas, R.J.; Chevallier, L.P. *Carte Géologique du Maroc: Taghdout-Echelle 1/50,000*; Notes et Mémoires du Service Géologique du Maroc N° 396; CGS South Africa: Pretoria, South Africa, 2000.
23. Middlemost, E.A. Naming materials in the magma/igneous rock system. *Earth-Sci. Rev.* **1994**, *37*, 215–224. [CrossRef]
24. Cox, K.; Bell, J.; Pankhurst, R. *The Interpretation of Igneous Rocks George*; Allen and Unwin: London, UK, 1979; p. 450.
25. Winchester, J.A.; Floyd, P.A. Geochemical discrimination of different magma series and their differentiation products using immobile elements. *Chem. Geol.* **1977**, *20*, 325–343. [CrossRef]
26. Perfit, M.R.; Gust, D.; Bence, A.E.; Arculus, R.; Taylor, S.R. Chemical characteristics of island-arc basalts: Implications for mantle sources. *Chem. Geol.* **1980**, *30*, 227–256. [CrossRef]
27. Bowen, N. *The Evolution of the Igneous Rocks*; Princeton University Press: Princeton, NJ, USA, 1928.
28. Peccerillo, A.; Taylor, S. Geochemistry of Eocene calc-alkaline volcanic rocks from the Kastamonu area, northern Turkey. *Contrib. Mineral. Petrol.* **1976**, *58*, 63–81. [CrossRef]
29. Irvine, T.N.; Baragar, W. A guide to the chemical classification of the common volcanic rocks. *Can. J. Earth Sci.* **1971**, *8*, 523–548. [CrossRef]
30. Cabanis, B.; Lecolle, M. Le diagramme La/10-Y/15-Nb/8: Un outil pour la discrimination des séries volcaniques et la mise en évidence des processus de mélange et/ou de contamination crustale. *C. R. Acad. Sci.* **1989**, *309*, 2023–2029.
31. Pearce, J.A. Trace element characteristics of lavas from destructive plate boundaries. In *Orogenic Andesites and Related Rocks*; John Wiley and Sons: Hoboken, NJ, USA, 1982; pp. 528–548.
32. Pearce, J.; Harris, N.B.; Tindle, A.G. Trace element discrimination diagrams for the tectonic interpretation of granitic rocks. *J. Pet.* **1984**, *25*, 956–983. [CrossRef]
33. Dupuy, C.; Dostal, J. Trace element geochemistry of some continental tholeiites. *Earth Planet. Sci. Lett.* **1984**, *67*, 61–69. [CrossRef]
34. McDonough, W.F.; Sun, S.-S. The composition of the Earth. *Chem. Geol.* **1995**, *120*, 223–253. [CrossRef]
35. Bertrand, H.; Dostal, J.; Dupuy, C. Geochemistry of early Mesozoic tholeiites from Morocco. *Earth Planet. Sci. Lett.* **1982**, *58*, 225–239. [CrossRef]

36. Vicat, J.-P.; Léger, J.-M.; Nsifa, E.; Piguet, P.; Nzenti, J.-P.; Tchameni, R. Distinction, au sein du craton congolais du sud-ouest du Cameroun, de deux épisodes doléritiques initiant les cycles orogéniques éburnéen (Paléoprotérozoïque) et panafricain (Néoprotérozoïque). *C. R. Acad. Sci.* **1996**, *323*, 575–582.
37. Thompson, R.; Morrison, M.; Hendry, G.; Parry, S. An assessment of the relative roles of crust and mantle in magma genesis: An elemental approach. *Philos. Trans. R. Soc. Lond.* **1984**, *310*, 549–590.
38. Winchester, J.; Floyd, P. Geochemical magma type discrimination: Application to altered and metamorphosed basic igneous rocks. *Earth Planet. Sci. Lett.* **1976**, *28*, 459–469. [CrossRef]
39. Thompson, A.B. Dehydration melting of pelitic rocks and the generation of H_2O-undersaturated granitic liquids. *Am. J. Sci.* **1982**, *282*, 1567–1595. [CrossRef]
40. Boyton, W. Geochemistry of the rare earth elements: Meteorite studies. In *Rare Earth Element Geochemistry*; Elsevier: Amsterdam, The Netherlands, 1984; pp. 63–114.
41. Saquaque, A.; Benharref, M.; Abia, H.; Mrini, Z.; Reuber, I.; Karson, J.A. Evidence for a Panafrican volcanic arc and wrench fault tectonics in the Jbel Saghro, Anti-Atlas, Morocco. *Geol. Rundsch.* **1992**, *81*, 1–13. [CrossRef]
42. Leblanc, M. *Ophiolites Précambriennes et Gites Arseniés de Cobalt: Bou Azzer (Maroc)*; Faculte des Science Paris VI, Memoires Centre Geologique et Geophysique: Paris, France, 1975.
43. Chabane, A.; El Boukhari, A.; Rocci, G.; TANE, J.-L. Découverte d'un magmatisme d'affinité boninitique d'arc associé à l'ophiolite panafricaine de Khzama (Massif du Siroua, Anti-Atlas marocain). *C. R. Acad. Sci.* **1991**, *313*, 1301–1304.
44. EL Boukhari, A.; Chabane, A.; Rocci, G.; Tane, J.-L. Le volcanisme de la région de N'Kob (SE du Siroua, Anti-Atlas marocain) témoin de l'existence d'un rift au Protérozoïque supérieur, à la marge NE du Craton ouest africain. *C. R. Acad. Sci.* **1991**, *312*, 735–738.
45. Admou, H. *Structuration de la Paléo Suture Ophiolitique Panafricaine de Bou Azzer-Siroua (Anti-Atlas Central, Maroc)*; Université Cadi Ayyad, Faculty of Sciences Semlalia: Marrakech, Morocco, 2000.
46. Sun, S.-S.; Nesbitt, R.W. Petrogenesis of Archaean ultrabasic and basic volcanics: Evidence from rare earth elements. *Contrib. Mineral. Petrol.* **1978**, *65*, 301–325. [CrossRef]
47. Sun, S.-S.; Nesbitt, R.W.; Sharaskin, A.Y. Geochemical characteristics of mid-ocean ridge basalts. *Earth Planet. Sci. Lett.* **1979**, *44*, 119–138. [CrossRef]
48. Le Roex, A.P.; Erlank, A.; Needham, H. Geochemical and mineralogical evidence for the occurrence of at least three distinct magma types in the 'Famous' region. *Contrib. Mineral. Petrol.* **1981**, *77*, 24–37. [CrossRef]
49. Le Roex, A.P. Geochemistry, mineralogy and magmatic evolution of the basaltic and trachytic lavas from Gough Island, South Atlantic. *J. Petrol.* **1985**, *26*, 149–186. [CrossRef]
50. Marcelot, G.; Dupuy, C.; Dostal, J.; Rancon, J.P.; Pouclet, A. Geochemistry of mafic volcanic rocks from the Lake Kivu (Zaire and Rwanda) section of the western branch of the African Rift. *J. Volcanol. Geotherm. Res.* **1989**, *39*, 73–88. [CrossRef]
51. Sun, S.-S.; McDonough, W.F. *Chemical and Isotopic Systematics of Oceanic Basalts: Implications for Mantle Composition and Processes*; Geological Society, London, Special Publications: London, UK, 1989; Volume 42, pp. 313–345. [CrossRef]
52. Morata, D.; Puga, E.; Demant, A.; Aguirre, L. Geochemistry and tectonic setting of the «ophites» from the external zones ofthe Betic Cordilleras (S. Spain). *Estudios Geol.* **1997**, *53*, 107–120. [CrossRef]
53. Ait Malek, H.; Gasquet, D.; Bertrand, J.-M.; Leterrier, J. Géochronologie U-Pb sur zircon de granitoïdes éburnéens et panafricains dans les boutonnières protérozoïques d'Igherm, du Kerdous et du Bas Drâa (Anti-Atlas occidental, Maroc). *C. R. Acad. Sci.* **1998**, *327*, 819–826.
54. Walsh, G.J.; Aleinikoff, J.N.; Benziane, F.; Yazidi, A.; Armstrong, T.R. U–Pb zircon geochronology of the Paleoproterozoic Tagragra de Tata inlier and its Neoproterozoic cover, western Anti-Atlas, Morocco. *Precambrian Res.* **2002**, *117*, 1–20. [CrossRef]
55. Hawkins, M.; Smith, M.; Powell, J.; Waters, C. *Carte Géologique du Maroc: Al YounDar a-Echelle 1/50,000*; Notes et Mémoires Du Service Géologique Maroc; Editeur British Geological Survey: Rabat, Morocco, 2001.
56. De Beer, C.; Chevallier, L.; De Kock, G.; Gresse, P.; Thomas, R. *Mémoire Explicatif de la Carte Géologique du Maroc au 1/50,000, Feuille Sirwa*; Notes et Mémoires Du Service Géologique Maroc; Editeur British Geological Survey: Rabat, Morocco, 2000; Volume 395, p. 86.
57. Saïdi, A.; Hafid, A.; Sagon, J.-P.; Julivert, M.; Arboleya, M.L.; Saquaque, A.; Rizki, A. La série de Zenaga (Anti-Atlas, Maroc): Pétrologie et structure des formations métamorphiques paléoprotérozoïques. *Géologie Méditerranéenne* **2001**, *28*, 203–221. [CrossRef]
58. Debon, F.; Le Fort, P. A chemical–mineralogical classification of common plutonic rocks and associations. *Earth Environ. Sci. Trans. R. Soc. Edinb.* **1983**, *73*, 135–149. [CrossRef]
59. Lameyre, J. Les magmas granitiques: Leurs comportements, leurs associations et leurs sources. *Mem. Hors Ser. Soc. Geol. Fr.* **1980**, *10*, 51–62.
60. Dostal, J.; Baragar, W.; Dupuy, C. Geochemistry and petrogenesis of basaltic rocks from Coppermine River area, Northwest Territories. *Can. J. Earth Sci.* **1983**, *20*, 684–698. [CrossRef]
61. Cox, K.; Hawkesworth, C. Geochemical stratigraphy of the Deccan Traps at Mahabaleshwar, Western Ghats, India, with implications for open system magmatic processes. *J. Petrol.* **1985**, *26*, 355–377. [CrossRef]
62. Cabanis, B.; Cochemé, J.; Vellutini, P.; Joron, J.; Treuil, M. Post-collisional Permian volcanism in northwestern Corsica: An assessment based on mineralogy and trace-element geochemistry. *J. Volcanol. Geotherm. Res.* **1990**, *44*, 51–67. [CrossRef]
63. Fitton, J.; Saunders, A.; Larsen, L.; Fram, M.; Demant, A.; Sinton, C.; Party, T. Magma sources and plumbing systems during break-up of the SE Greenland margin: Preliminary results from ODP Leg 152. *J. Geol. Soc.* **1995**, *152*, 985–990. [CrossRef]

64. Hildreth, W.; Halliday, A.N.; Christiansen, R.L. Isotopic and chemical evidence concerning the genesis and contamination of basaltic and rhyolitic magma beneath the Yellowstone Plateau volcanic field. *J. Petrol.* **1991**, *32*, 63–138. [CrossRef]
65. Hofmann, A.W.; Jochum, K.P.; Seufert, M.; White, W.M. Nb and Pb in oceanic basalts: New constraints on mantle evolution. *Earth Planet. Sci. Lett.* **1986**, *79*, 33–45. [CrossRef]
66. Taylor, S.R.; McLennan, S.M. *The Continental Crust: Its Composition and Evolution*; Blackwell Scientific Publications: Oxford, UK, 1985.
67. Alibert, C. A Sr-Nd isotope and REE study of Late Triassic dolerites from the Pyrenees (France) and the Messejana Dyke (Spain and Portugal). *Earth Planet. Sci. Lett.* **1985**, *73*, 81–90. [CrossRef]
68. Dupuy, C.; Marsh, J.; Dostal, J.; Michard, A.; Testa, S. Asthenospheric and lithospheric sources for Mesozoic dolerites from Liberia (Africa): Trace element and isotopic evidence. *Earth Planet. Sci. Lett.* **1988**, *87*, 100–110. [CrossRef]
69. Hafid, A. *Granites et Dolérites Protérozoïques de la Boutonnière d'Irherm (Anti-Atlas Occidental, Maroc):(Pétrologie, Géochimie et Signification Géodynamique)*; Universite Pierre et Marie Curie, Paris VI: Paris, France, 1992.
70. Irving, E.; Baker, J.; Hamilton, M.; Wynne, P. Early Proterozoic geomagnetic field in western Laurentia: Implications for paleolatitudes, local rotations and stratigraphy. *Precambrian Res.* **2004**, *129*, 251–270. [CrossRef]
71. Gladkochub, D.P.; Pisarevsky, S.A.; Donskaya, T.V.; Ernst, R.E.; Wingate, M.T.; Söderlund, U.; Mazukabzov, A.M.; Sklyarov, E.V.; Hamilton, M.A.; Hanes, J.A. Proterozoic mafic magmatism in Siberian craton: An overview and implications for paleocontinental reconstruction. *Precambrian Res.* **2010**, *183*, 660–668. [CrossRef]
72. Charlot, R. *Caractérisation des Événements Éburnéens et Panafricains dans l'Anti-Atlas Marocain: Apport de la Méthode Géochronologique Rb-Sr*; Editions du Service géologique du Maroc: Rabat, Morocco, 1982.

Disclaimer/Publisher's Note: The statements, opinions and data contained in all publications are solely those of the individual author(s) and contributor(s) and not of MDPI and/or the editor(s). MDPI and/or the editor(s) disclaim responsibility for any injury to people or property resulting from any ideas, methods, instructions or products referred to in the content.